

The VMC Survey - XXXVII. Pulsation periods of dust enshrouded AGB stars in the Magellanic Clouds ★ ★★

M. A. T. Groenewegen¹, A. Nanni², M. -R. L. Cioni³, L. Girardi⁴, R. de Grijs^{5,6,7}, V. D. Ivanov⁸, M. Marconi⁹,
M.-I. Moretti⁹, J. M. Oliveira¹⁰, M. G. Petr-Gotzens^{8,11}, V. Ripepi⁹, and J. Th. van Loon¹⁰

¹ Koninklijke Sterrenwacht van België, Ringlaan 3, B-1180 Brussels, Belgium
e-mail: martin.groenewegen@oma.be

² Aix Marseille Université, CNRS, CNES, LAM, 38, rue Frédéric Joliot-Curie, F-13388 Marseille, Cedex 13 France

³ Leibniz Institut für Astrophysik Potsdam, An der Sternwarte 16, D-14482 Potsdam, Germany

⁴ Osservatorio Astronomico di Padova-INAf, Vicolo dell'Osservatorio 5, I-35122 Padova, Italy

⁵ Department of Physics and Astronomy, Macquarie University, Balaclava Road, Sydney, NSW 2109, Australia

⁶ Research Centre for Astronomy, Astrophysics and Astrophotonics, Macquarie University, Balaclava Road, Sydney, NSW 2109, Australia

⁷ International Space Science Institute–Beijing, 1 Nanertiao, Zhongguancun, Hai Dian District, Beijing 100190, China

⁸ European Southern Observatory, Karl-Schwarzschild-Str. 2, D-85748 Garching bei München, Germany

⁹ INAF – Osservatorio Astronomico di Capodimonte, via Moiariello 16, I-80131, Naples, Italy

¹⁰ Lennard-Jones Laboratories, School of Chemical and Physical Sciences, Keele University, ST5 5BG, UK

¹¹ Universitäts-Sternwarte, Ludwig-Maximilians-Universität München, Scheinerstr 1, D-81679 München, Germany

received: 2019, accepted: 2020

ABSTRACT

Context. Variability is a key property of stars on the asymptotic giant branch (AGB). Their pulsation period is related to the luminosity and mass-loss rate of the star. The long-period variables (LPVs) and Mira variables are the most prominent of all types of variability of evolved stars. The reddest, most obscured AGB stars are too faint in the optical and have eluded large variability surveys.

Aims. Obtain a sample of LPVs by analysing *K*-band light-curves (LCs) of a large number of sources in the direction of the Magellanic Clouds with the colours expected for red AGB stars ($(J - K) > 3$ mag or equivalent in other colour combinations).

Methods. Selection criteria are derived based on colour-colour and colour-magnitude diagrams from the combination of VISTA Magellanic Cloud (VMC) survey, *Spitzer* IRAC and AllWISE data. After eliminating LPVs with known periods shorter than 450 days, a sample of 1299 candidate obscured AGB stars is selected. *K*-band LCs are constructed combining the epoch photometry available in the VMC survey with literature data, analysed for variability and fitted with a single period sine curve to derive mean magnitudes, amplitudes and periods. A subset of 254 stars are either new variables, or known variables where the period we find is better determined than the literature value, or longer than 1000 days. The spectral energy distributions (SEDs) of these stars are fitted to a large number of templates. For this purpose the SEDs and *Spitzer* IRS spectra of some non-AGB stars (Be stars, HII regions and young stellar objects [YSOs]) are also fitted to have templates of the most likely contaminants in the sample.

Results. A sample of 217 likely LPVs is found. Thirty-four stars have periods longer than 1000 days although some of them have alternative shorter periods. The longest period of a known Mira in the Magellanic Clouds from Optical Gravitational Lensing Experiment (OGLE) data (with $P = 1810$ d) is derived to have a period of 2075 d based on its infrared LC. Two stars are found to have longer periods, but both have lower luminosities and smaller pulsation amplitudes than expected for Miras. Mass-loss rates and luminosities are estimated from the template fitting. Period-luminosity relations are presented for C- and O-rich Miras that appear to be extensions of relations derived in the literature for shorter periods. The fit for the C-stars is particularly well defined (with 182 objects) and reads $M_{\text{bol}} = (-2.27 \pm 0.20) \cdot \log P + (1.45 \pm 0.54)$ mag with an rms of 0.41 mag. Thirty-four stars show pulsation properties typical of Miras while the SEDs indicate they are not. Overall, the results of the LC fitting are presented for over 200 stars that are associated to YSOs.

Key words. Magellanic Clouds – Stars: AGB and post-AGB – Stars: variables: general – Infrared: general

1. Introduction

At the end of their lives essentially all low- and intermediate mass stars (roughly ~ 0.9 to $\sim 10 M_{\odot}$ on the main sequence) will go through the (super)-asymptotic giant branch (AGB) phase.

Send offprint requests to: Martin Groenewegen

* Tables A.1, A.2, A.3, and D.1 are available in electronic form at the CDS via anonymous ftp to cdsarc.u-strasbg.fr (130.79.128.5) or via <http://cdsweb.u-strasbg.fr/cgi-bin/qcat?J/A+A/>. Figures A.1 and C.2 are available in the on-line edition of A&A.

** Based on observations made with VISTA at ESO under programme ID 179.B-2003.

They end up as $\sim 0.55 - 1.4 M_{\odot}$ white dwarfs which means that a large fraction of the initial mass of the star is lost to the interstellar medium. An important characteristic of AGB stars is that they pulsate, classically divided into stars with small amplitudes (the semi-regular variables, SRVs) and the large amplitude Mira variables. It is now common to use the term long period variable (LPV) irrespective of pulsation amplitude for a pulsating star on the AGB. Pulsation-induced shock waves and radiation pressure on dust is the most promising mechanism to explain wind driving, especially regarding the more evolved AGB stars with low effective temperatures, large pulsation amplitudes, and high

mass-loss rates (MLRs; see the review by Höfner & Olofsson 2018).

It was known from observations in the Large Magellanic Cloud (LMC) that Miras follow a period-luminosity (*PL*) relation (Glass & Evans 1981; Feast et al. 1989), but the breakthrough came with the advent of micro-lensing surveys. Wood et al. (1999) and Wood (2000) showed that late-type stars in the LMC followed 5 sequences (labelled A, B, C, D and E). Subsequent work demonstrated that sequence B consists actually of two sequences (B and C') and that there exists an additional sequence (A'), including possible substructure (Ita et al. 2004; Soszyński et al. 2007). Sequence D consists of long secondary periods (LSPs), while sequence E is due to binary stars. A theoretical interpretation using linear, radial, non-adiabatic pulsation models and a population synthesis model show that sequences A', A, B + C', and C, correspond to third, second, first overtone, and fundamental mode pulsation, respectively (Trabucchi et al. 2017). The LPVs with the largest amplitudes, the classical Miras, dominate sequence C.

The Mira *PL*-relation has been used as a distance indicator, traditionally inside the Milky Way galaxy in the pre-*Gaia* era (e.g. Groenewegen et al. 2002; Ramstedt & Olofsson 2014). The method has gained recent interest in the context of the distance ladder as an independent check on Cepheid or tip of the red giant branch distances, for example recent works on the megamaser galaxy NGC 4258 (Huang et al. 2018) or the SN host galaxy NGC 1559 (Huang et al. 2020). As Miras are as bright as Cepheids in the NIR they will be important secondary calibrators in the upcoming era of ground-based extremely large telescopes and the *James Webb Space Telescope*.

The currently largest survey of LPVs in the Magellanic Clouds (MCs) is the Optical Gravitational Lensing Experiment OGLE-III catalogue, which contains 1667 Mira stars, 11 128 SRVs and 79 200 OGLE Small Amplitude Red Giants (OSARGs) in the LMC (Soszyński et al. 2009a), and 352 Mira stars, 2222 SRVs and 16 810 OSARGs in the Sarge Magellanic Cloud (SMC) (Soszyński et al. 2011).

However, OGLE and other current surveys in the optical domain will miss the reddest, most obscured AGB stars. At the very end of the AGB the (dust) MLR may become so large that the object becomes very faint, beyond the OGLE *I*-band detection limit of about 21 mag. The dust grains in the circumstellar envelope (CSE) scatter and absorb the emission in the optical to re-emit it in the near- and mid-infrared (NIR, MIR).

These stars are known to exist in the LMC. They were typically selected as having *Infrared Astronomical Satellite* (IRAS) colours similar to obscured AGB stars in our Galaxy. Wood et al. (1992) give periods for 9 sources in the LMC. Periods range between 930 and 1390 d, with peak-to-peak amplitudes in *K* between 0.3 and 2.1 mag, and (*J* − *K*) colours that range from 2.1 to 5.7 mag (an additional 7 LMC and 3 SMC sources were monitored but showed small amplitudes and no periods were given). Wood (1998) monitored 12 sources and 9 turned out to be LPVs with periods in the range 530 to 1295 d. Amplitudes in *K* are between 0.85 and 1.9 mag, and colours range from (*J* − *K*) = 3.9 to 6.1 mag (with two not detected in *J*). Similarly, Whitelock et al. (2003) give periods for two dozen stars which have an IRAS identifier. Periods range from 540 to 1390 days, *K*-band amplitudes are between 0.52 and 1.8 mag, and (*J* − *K*) colours range from 1.9 to 4.0 mag (with several not detected in *J*). The faintest stars in these works have (mean light) magnitudes in the range *K* = 12 − 13 mag.

The ESO public VISTA Magellanic Cloud (VMC) survey is a photometric survey in three filters, *Y*, *J*, and *K_s* performed at

the VISTA telescope using the VIRCAM camera. The latter provides a spatial resolution of 0.34'' per pixel and a non-contiguous field-of-view of 1.65 deg² sampled by 16 detectors. To homogeneously cover the field-of-view it is necessary to fill these gaps using a six-point mosaic. This is the unit area of VISTA surveys called a tile and covers uniformly with at least two exposures per pixel an area of 1.5 deg² (Emerson & Sutherland 2010).

The VMC survey covers an area of approximately 170 deg² (110 tiles) of the MC system and includes stars as faint as 22 mag in *K_s* (5σ, Vega mag), see Cioni et al. (2011) for description of the survey. The large areal coverage and the survey depth are the main strengths of the VMC survey compared to earlier works in the IR. Unlike the VMC papers on classical variables (Type-II and Classical Cepheids, RR Lyrae, e.g. Ripepi et al. 2012, 2015, 2016, 2017; Muraveva et al. 2018) the expected periods for AGB pulsators are much longer than the baseline of the VMC observations. Therefore the VMC data is combined with *K*-band data from the literature when available to increase the time span.

In the present paper *K*-band light-curves (LCs) are inspected for a large number of candidate dust-obscured AGB stars. The sample is selected based on colour-magnitude and colour-colour criteria derived from the properties of known AGB stars, using both VMC and other infrared data.

The paper is organised as follows. Section 2 discusses how the sample of potential LPVs is selected based on different photometric catalogues, and the creation of the *K*-band LCs. Section 3 discusses how the LCs are analysed. Section 4 discusses the results. The sample of potential LPVs is further reduced by considering the shape of the spectral energy distributions (SEDs).

Preliminary results of this work were shown or used in Groenewegen et al. (2016), Cioni et al. (2017) and Groenewegen & Sloan (2018) (hereafter GS18) but the results on the LC parameters are superseded by this paper.

2. Sample selection

In this section the sample of candidate obscured AGB stars is generated. It is based on three different photometric catalogues. The first selection uses only VMC data¹, but requires a detection in *J* and *K_s* for reliability (sample 1). The second selection combines the VMC *K_s*-band data with *WISE* data from the All-*WISE* catalogue (Cutri et al. 2013) (sample 2). The third selection starts with data exclusively from the Surveying the Agents of a Galaxy's Evolution (SAGE) survey of the MCs, and then looks for a possible counterpart in the VMC data (sample 3). During this selection procedure only the mean magnitudes as given by the VISTA Science Archive (VSA; Cross et al. 2012) are used, and the quality flags indicating warnings and possible issues (the *ppErrBits*) are not considered. Only in the second step is the time-resolved VMC *K_s*-band data used and combined with literature data to produce a LC.

2.1. Sample 1: VMC data only

Figure 1 shows the VMC (*K_s*, (*J* − *K_s*)) colour-magnitude diagram (CMD) for a region in the Bridge between the two Clouds, and a region located in the bar of the LMC. The region in the Bridge is used to delineate the locus in colour space occupied by extended objects, most of which are background galaxies but

¹ All VMC data refers to observations obtained until the end of September 2016, including complete observations of the Small Magellanic Cloud.

that can also result from blends (colour coded in red)², while the region in the bar shows the well-known sequence of AGB stars redder than $(J - K_s) \sim 1.5$ mag at relatively bright magnitudes. At the brightest level ($K_s \lesssim 10.5$ mag) one notices the effect of saturation. This is not expected to influence the selection of obscured AGB stars for which the distribution in the CMD bends to faint magnitudes. This is shown more clearly in Fig. 2.

In a subsequent step all (about 7000) stars in VMC with a detection in J and K_s , $(J - K_s) > 1.5$ mag, and $K_s < 3 \cdot (J - K_s) + 10$ mag were selected to represent candidate obscured AGB stars. Their CMD distribution is shown in the left-hand panel of Fig. 2, and shows that there is still an important contribution by background galaxies and other extended objects. This CMD also clearly exhibits the sequence of increasing mass loss along the AGB. A fit is made to this sequence, $K_s = 10.318 + 0.287 \cdot (J - K_s) + 0.0306 \cdot (J - K_s)^2$ mag, and this relation shifted by 2 magnitudes to fainter magnitudes to delineate the approximate lower boundary of this sequence, is shown as well.

Another consideration in selecting the stars is that the primary interest is in studying the reddest pulsating AGB stars, objects that are too faint for the current optical surveys like OGLE-III and OGLE-IV, that have a limiting magnitude in the I -band around 20-21 mag.

GS18 fitted the SEDs and spectra taken with the *Spitzer* Infrared Spectrograph (IRS, Houck et al. 2004) spectra of almost 400 AGB and red supergiant (RSG) stars in the MCs, and determined periods for a large fraction of them. The periods were derived by analysing existing optical data (from the OGLE, Massive Compact Halo Objects (MACHO), and Expérience de Recherche d'Objets Sombres (EROS) surveys), or data in the K and K_s bands (including VMC data) and in the *WISE* W2 band for the reddest objects.

The right-hand panel of Fig. 2 shows the I , $(J - K_s)$ CMD for about 150 O- and C-rich AGB stars in the MCs with a pulsation period longer than 450 days, based on synthetic photometry, that is, the simulated magnitudes taking into account the filter transmission curves and photometric zero points in many filters using the best-fitting model to the SEDs in GS18. Marked in red are stars where the pulsation period is based on K/K_s or W2 data, the other periods are derived from optical data (mainly OGLE). The diagram shows that the I -band limit of 20 mag is reached for stars that have a $(J - K_s)$ colour of ~ 4 mag.

To have sufficient overlap with the optical surveys, and to be on the conservative side, a limit of $(J - K_s) = 3$ mag is chosen. Sample 1 consists of the 857 stars in the VMC survey that have a detection in J and K_s , $(J - K_s) > 3$ mag and $K_s < 12.318 + 0.287 \cdot (J - K_s) + 0.0306 \cdot (J - K_s)^2$ mag.

2.2. Sample 2: VMC and WISE data combined

While sample 1 has the advantage that it uses exclusively data from the VMC survey, the reddest AGB stars, by their very nature, will become J -band dropouts for large enough MLRs. The aim of constructing samples 2 and 3 is to combine VMC K_s -band data with data at longer wavelengths, in particular *WISE* (sample 2), or IRAC (sample 3). The advantage of *WISE* is that it is an all-sky survey, covering the complete area observed by the VMC survey.

The AllWISE catalogue (Cutri et al. 2013) is available as a table in the VSA and the queries were therefore performed

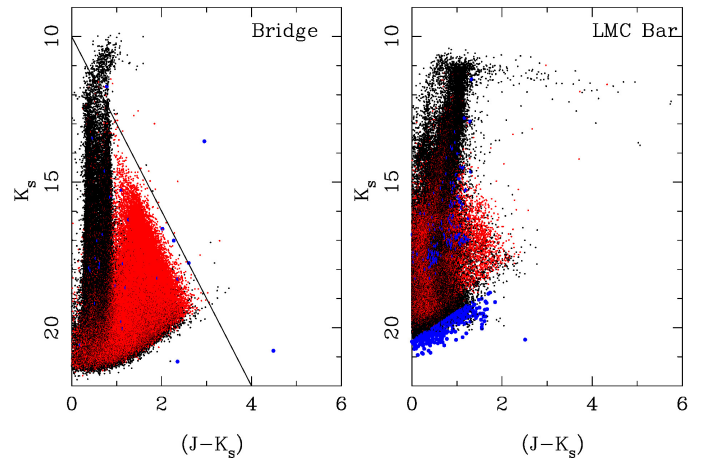


Fig. 1. VMC (K_s , $(J - K_s)$) CMD in a region in the Magellanic Bridge (left-hand panel; a strip at $42^\circ < \text{R.A.} < 52^\circ$ and $-72.5^\circ < \text{Dec.} < -73.8^\circ$) and in the LMC bar (right-hand panel; a box defined as $80^\circ < \text{R.A.} < 82^\circ$, and $-69^\circ < \text{Dec.} < -70^\circ$). Objects that are (probable) stars are indicated in black, and (probable) galaxies (extended objects) are indicated in red. Objects classified differently are indicated in blue. The line, $K_s = 3 \cdot (J - K_s) + 10$ mag, indicates the approximate boundary of galaxies.

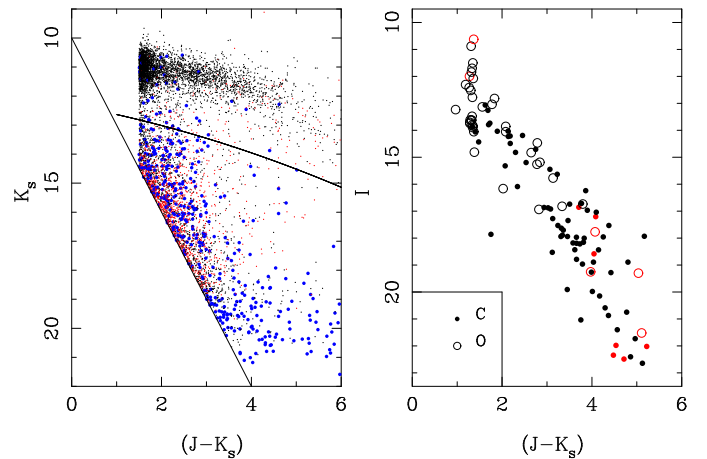


Fig. 2. Left-hand panel: All VMC stars with a detection in J and K_s , redder than $(J - K_s) = 1.5$ mag, and above the line $K_s = 3 \cdot (J - K_s) + 10$ mag. The second-order polynomial is a fit to the red sequence of AGB stars, shifted downward by 2 magnitudes for comparison purposes (see text). Objects that are (probable) stars are indicated in black, and (probable) galaxies are indicated in red. Objects classified differently are indicated in blue. Right-hand panel: Synthetic photometry from GS18 for 29 SMC and 133 LMC O- (open circles) and C-rich (filled circles) AGB stars with pulsation periods longer than 450 days. The objects marked in red have pulsation periods derived from K/K_s or *WISE*-band data, the black points from optical data (OGLE, EROS, MACHO).

within the VSA. A search radius of $1''$ was used and an error on the $W1$ magnitude of less than 0.2 mag was imposed (equivalent to $w1snr > 5$).

The left-hand panel of Fig. 3 shows the $(W1, K_s - W1)$ CMD for a region in the Bridge, with the same colour coding for background galaxies and stars as in Fig. 1. The line $W1 = 1.0 \cdot (K_s - W1) + 10.5$ indicates the approximate boundary beyond which (at bright magnitudes and red colours) the number of galaxies significantly decreases. In the second panel all sources are shown which have $(K_s - W1) > 1$ mag, $(W1 - W2) > 0.5$ mag, and are brighter than this boundary. The corresponding colour-

² Indicated by the *mergedClass* parameter which is -9 for a saturated source, -3 for a probable galaxy, -2 for a probable star, -1 for a star, 0 for noise, and $+1$ for a galaxy.

colour diagram (CCD) is shown in the bottom half of the right-most panel.

The third panel from the left shows a synthetic CMD based on the AGB stars studied by GS18. The line $W1 = 0.7 \cdot (K_s - W1) + 10.0$ is the empirical conservative lower boundary to the reddest AGB stars, and is also shown in the second panel from the left. The corresponding CCD is shown in the top-half of the right-most panel with the lines $(W1 - W2) = 0.8$ mag and $(W1 - W2) = 0.37 \cdot (K_s - W1) - 0.2$ mag.

The final selection is based on a detection in K_s , a signal-to-noise ratio (SNR) in the $W1$ band > 5 , $(W1 - W2) > 0.8$ mag, $W1 < 0.7 \cdot (K_s - W1) + 10.0$ mag, and $(W1 - W2) > 0.37 \cdot (K_s - W1) - 0.2$ mag for a total of 1317 sources.

2.3. Sample 3: SAGE data first

SAGE (Meixner et al. 2006) and SAGE-SMC (Gordon et al. 2011) are surveys of the LMC and SMC with the *Spitzer* telescope. The advantage of *Spitzer* is that it has a smaller point-spread-function than *WISE*, and confusion is less of an issue. On the other hand the SAGE observations do not cover entirely the area sampled by the VMC survey. The combined LMC and SMC source catalogue in the [3.6], [4.5], [5.8], and [8.0] bands is available electronically³.

Figure 4 shows in the left panel the ([8.0], [3.6]–[8.0]) CMD of all sources with detections in all four bands. The region occupied by background galaxies is clearly visible, as well as a tail of bright red AGB stars.

Boyer et al. (2011) used this diagram to select very red AGB stars, and we follow their work in selecting stars with $[3.6] - [8.0] > 0.8$ mag. Our elimination of background galaxies is less conservative than theirs, and we select objects above the line $[8.0] < 13.0 - ([3.6] - [8.0])$ (for $[3.6] - [8.0] < 4$ mag), and $[8.0] < 9.0 + ([3.6] - [8.0] - 4.0)$ mag for redder objects.

The $([3.6] - [4.5], [5.8] - [8.0])$ CCD of sources that meet these conditions is plotted in the top of the right-hand panel of Fig. 4. The bottom panel shows the synthetic photometry based on GS18; a region delineated by the lines $[3.6] - [4.5] > -0.6 \cdot ([5.8] - [8.0]) + 0.6$ (for $([5.8] - [8.0]) < 1$ mag), and $[3.6] - [4.5] > 1.7 \cdot ([5.8] - [8.0]) - 1.7$ (for $([5.8] - [8.0]) > 1$ mag) is defined. The initial sample consists of 1958 SAGE sources that meet these constraints.

The next step is the correlation with the VMC database. After inspecting the results using a search radius of $1''$ the final correlation was done returning all VMC counterparts within $0.8''$ of the SAGE coordinates. Ten sources had multiple counterparts listed, but in all cases there was no reason not to take the closest match. In the sample 35 SAGE stars had no counterpart in VMC, and in eight cases the counterpart lacked K_s -band data, leaving 1915 objects.

The selection so far was based on SAGE colours, and positions. An additional consistency check between the IRAC and the K_s -band VMC magnitude is performed. Based on the synthetic photometry from GS18 we impose a limit of $K_s - [3.6] > 1.5$ mag (which is consistent with the limit $(J - K_s) > 3$ mag in selecting sample 1). This removes over 300 sources for a final sample size of 1562.

2.4. The final sample

2.4.1. Sample statistics

The three samples were combined and together contain 2014 unique sources. This sample is almost of the same size as that of the known Mira population in the MCs, indicating that the initial sample selection based on colour criteria has not been very restrictive.

As the main interest in the present paper is in finding new (red, [very] long-period) pulsating stars, the next step is a correlation with lists of known LPVs. To be able to compare the properties (in terms of period, amplitude, etc.) of known Miras and LPVs with the new objects, known LPVs with periods longer than 450 days are kept, while LPVs with shorter periods are removed. This is an arbitrary choice but a good compromise, because including stars with shorter periods would increase the sample by including stars that would essentially never become optically obscured and where the period from the relatively poorly sampled IR LC would never be able to compete in quality with period(s) determined from OGLE data. At the same time the cut at 450 days allows overlap with OGLE to verify our procedures and compare periods and amplitudes.

A comparison with the OGLE-III catalogue of LPVs in the LMC (Soszyński et al. 2009a) and SMC (Soszyński et al. 2011) removes about 450 stars, and keeps about 480 LPVs with periods longer than 450 days. Similar correlations were done with the list of MACHO detected LPVs in the LMC (Fraser et al. 2008), and the catalogues of LPVs detected in the EROS-2 survey (Spano et al. 2011; Kim et al. 2014).

2.4.2. Light curves

The final sample of stars for which the LCs were analysed contains 1299 objects and for those the K_s -band epoch data were retrieved from the VSA archive. The information for all these objects is given in Appendix A. Table A.1 lists general information on the objects: the right ascension and declination (from VMC, all epochs in this paper are J2000), some common names and object type (from SIMBAD⁴), (selected) spectral types (from Skiff 2014), the variability-type as listed in the 2nd *Gaia* data release (GDR2, *Gaia* Collaboration et al. 2018; Holl et al. 2018), and the classification based on the MIR *Spitzer* IRS spectrum; see the footnote to the table for more information. Table A.2 lists known periods and related information from the literature, while Table A.3 lists the results of the period analysis (see Sect. 3 for details).

The LCs consist of the VMC K_s -band data with K/K_s -band data found in the literature added (as detailed in columns 7 and 8 of Table A.3). For some of the brightest stars the VMC photometry is influenced by non-linearity or saturation. A correction is applied in the VISTA pipeline for this (Irwin 2009) but for the brightest stars it does not correct sufficiently. In the LC fitting this was accounted for by shifting the VMC K_s -band photometry to externally available photometry (see the remarks in Column 10 of Table A.3). The shift was determined from the difference in the median of the VMC and the external photometry. The shifted VMC photometry was also assigned an error bar of 0.25 mag.

No attempt was made to bring the various K -band measurements onto a common system. The main reason is that colour transformations from one system to another almost always depend on the $(J - K)$ -colour (Carpenter 2001; Koen et al. 2007).

³ ViZieR catalogue II/305/archive

⁴ As of January 2019.

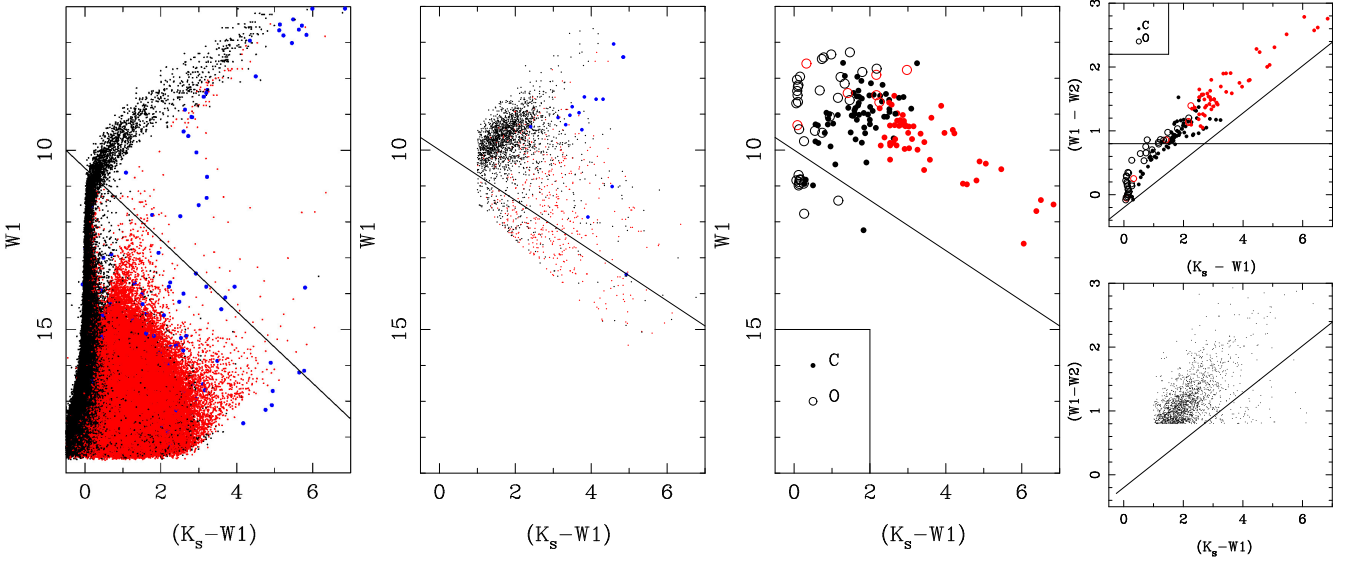


Fig. 3. WISE-VMC ($W1, K_s - W1$) CMD and $(W1 - W2) - (K_s - W1)$ CCDs. In the left-most panel the CMD in a region between the SMC and LMC (a strip at $30^\circ < \text{R.A.} < 60^\circ$) is presented. The line $W1 = 1.0 \cdot (K_s - W1) + 10.5$ mag indicates the upper boundary of the region predominantly occupied by galaxies. In the second panel from the left all WISE-VMC sources are shown which are brighter than the boundary line in the left-hand panel, $(K_s - W1) > 1$ mag and $(W1 - W2) > 0.5$ mag. Objects that are (probable) stars are indicated in black, and (probable) galaxies (extended objects) are indicated in red, while objects classified differently are indicated in blue in these two panels. The provenance of the line in the second panel is explained in the next panel. The corresponding CCD is shown in the bottom half of the right-most panel. The third panel from the left shows a synthetic CMD based on GS18 for 29 SMC and 133 LMC O- (open circles) and C-rich (filled circles) AGB stars with pulsation periods longer than 450 days. The objects marked in red have pulsation periods derived from K/K_s or *WISE*-band data, the black points from optical data (OGLE, EROS, MACHO). The line $W1 = 0.7 \cdot (K_s - W1) + 10.0$ mag is the empirical lower boundary to the reddest AGB stars, and is also shown in the second panel from the left. The corresponding CCD diagram is shown in the top-half of the right-most panel with the lines $(W1 - W2) = 0.8$ mag and $(W1 - W2) = 0.37 \cdot (K_s - W1) - 0.2$ mag, which indicates the empirical lower boundary to the reddest AGB stars, and is also shown in the panel below it.

A *J*-band magnitude observed simultaneously with the *K*-band data is not always available, the error on the *J*-band magnitude is typically large for these red sources, and the $(J - K)$ -colour is outside the range considered in the transformation formula. This would make a colour transformation particularly complicated and uncertain in many cases. This is a limitation, and in Appendix B we estimated the possible effect and come to the conclusion that it is typically smaller than the error bar quoted for mean magnitudes, amplitudes and periods in Table A.3. In the following text we refer to the *K*-band for simplicity unless we address a specific survey.

3. Modelling

The automatic analysis of the LCs is done with the Fortran codes available in *numerical recipes* (Press et al. 1992) as described in Appendix A of Groenewegen (2004). The codes were tuned at that time to analyse OGLE-II LCs with hundreds of data points, while the current LCs have between 6 and 73 data points (92% of the stars in the sample have 15 or more data points). This makes the determination of the pulsation period through Fourier analysis (using the subroutine *FASPER*) more complicated. Therefore the LCs of most stars in the sample were analysed manually with the code *PERIOD04* (Lenz & Breger 2005) as well. Once an initial guess of the period was determined (either through the automatic routine, a period found in the literature, or from the manual fitting of the LC) a function of the form

$$K(t) = K_0 + A \sin(2\pi t e^f) + B \cos(2\pi t e^f) \quad (1)$$

was fitted to the LC using the weighted linear least-squares fitting routine *MRQMIN*. This results in the parameters listed in Table A.3, mean magnitudes, periods ($\exp(-f)$), and amplitudes

($\sqrt{A^2 + B^2}$) with their associated uncertainties. Equation 1 implies that the LC can be described by a single period. It is well known that the LCs of LPVs are not strictly single-periodic. The OGLE team typically fits three periods to the LC. However with the limited number of data points available in the IR LCs we are not able in general to comment on the presence of more than one period. The exception is the few stars that have been monitored extensively from the ground. Table A.3 sometimes lists a long secondary period (LSP). Those were derived from the manual fitting of the LC using *PERIOD04*.

When no initial period is known from the literature it is taken from the Fourier analysis. The reliability of this period determination (also) depends on the number of data points in the LC. Selecting from Table A.3 those stars that have no initial period listed, and a $S/N > 3$ on the final period and amplitude shows that the minimum number of useable data points is 12.

A comparison of the LC with the fit sometimes suggested that alternative periods may be possible as well. These cases were inspected by manual fitting of the LC using *PERIOD04*, and alternative periods are sometimes indicated in Col. 9 of Table A.3.

The table also includes the reduced χ^2 , defined as $\chi_r^2 = \sum_i ((m_i - o_i)/\sigma_{o_i})^2 / (N - N_p)$, with m , o and σ_o indicating the model magnitude, the observed magnitude, and the error, N is the number of data points, and $N_p = 1$ or 4, depending on whether Eq. 1 is fitted without or with the period. The χ_r^2 in Table A.3 ranges from 0.2 to 3900, with a median of 70. These values are very large compared to an expected value of unity in case of a model describing the data correctly and with correct estimates of the error bars. This probably indicates that the internal error bars of the K_s -band photometry in the VSA (typically at the mmag

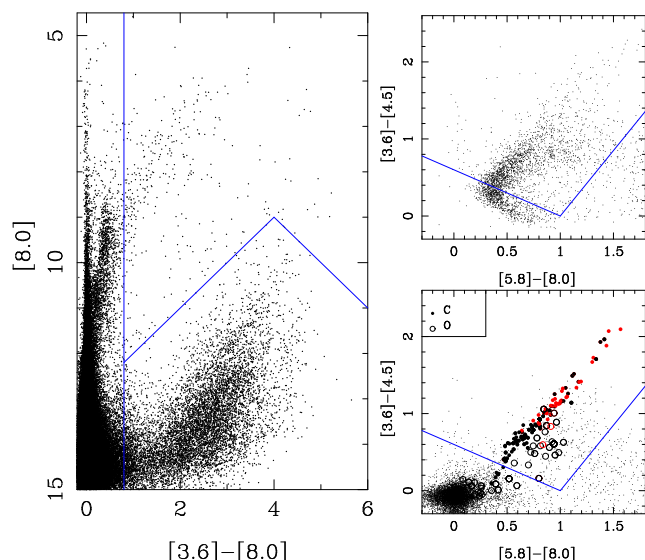


Fig. 4. Left-hand panel: the $([8.0], [3.6] - [8.0])$ CMD of LMC and SMC objects in the SAGE survey. Only every 10th star is plotted. The line at $[3.6] - [8.0] = 0.8$ mag indicates the blue limit of red AGB stars, and the two other lines indicate the limits of the region occupied mainly by background galaxies (see text). The top right-hand panel shows the $([3.6] - [4.5], [5.8] - [8.0])$ CCD of all sources that are located in the upper right of the CMD delineated by these lines. The bottom right-hand panel shows the same diagram with synthetic CCD based on GS18 for 29 SMC and 133 LMC O- (open circles) and C-rich (filled circles) AGB stars with pulsation periods longer than 450 days. The objects marked in red have pulsation periods derived from K/K_s or *WISE*-band data, the black points from optical data (OGLE, EROS, MACHO). The background sources in this panel are randomly picked from the S^3MC survey (Bolatto et al. 2007).

level) are likely underestimated when compared to other photometry on an absolute external scale, but also that differences in filter curves between the different sets of photometry, and the simplicity of the model (a single period) play a role. In the next section a selection is done eliminating stars with a $\chi_r^2 > 430$, which represents about 10% of the sample.

4. Analysis and selection of new red LPVs

4.1. Comparison to known Miras

The next step is a comparison of the results of the IR LC fitting to the periods of known Miras from OGLE-III. To compare between the OGLE and the IR pulsation properties we selected from Table A.2 the stars classified by OGLE to be Miras and with an amplitude for the second listed period smaller than that listed for the primary period (as given by OGLE). As mentioned above, many LPVs show a LSP, sometimes with a large amplitude, and this choice makes a more direct comparison of periods and amplitudes possible. After removing three stars for which the present analysis reveals no significant period there remain 294 stars to make the comparison, and the results are shown in Figure 5. The panel on the left compares the primary period found by OGLE to the period derived in the present work. The dotted line marks the one-to-one relation and shows that the agreement is very good in most cases. The middle panel compares the amplitudes in the K -band as found in our analysis with the amplitude in the I -band as found by OGLE. There is no strong correlation. One observes the cut-off in I -band amplitude that reflects the common definition (as used also by the

OGLE team) that Miras should have an I -band amplitude larger than 0.9 mag. The solid line is plotted to guide the eye and indicates an amplitude in K that is half that in I . The right-hand panel shows the relative error in the period determination plotted against period. The majority of stars have a period determination better than a few percent. The middle and right-hand panels identify outliers by the red symbols, stars where the amplitude is ill-defined (the error on the amplitude being larger than the amplitude itself), and by plus signs where the χ_r^2 in the LC fitting is > 430 . Using the following selection criteria 291 of the 294 known Miras (based on I -band data) with low amplitude secondary periods are selected:

- error in the period determination better than 4%.
- error in the amplitude smaller than the amplitude.
- amplitude larger than 0.1 mag in the K -band.
- χ_r^2 in the LC fitting procedure smaller than 430.

When these criteria are applied to the full sample (and also enforcing $P > 100$ days to eliminate a few known Type-II Cepheids) there are 634 objects of the 1299 that show pulsation properties as derived from the IR LCs consistent with those of known Miras (as defined based on I -band data). This includes the 291 stars that were used to define the criteria, but also known OGLE LPVs that were not used in the comparison (those with larger LSP amplitudes). In addition there are objects where the classification of the *Spitzer* IRS spectrum indicates that they are not AGB stars (see Table A.1). The amplitude cut-off of 0.1 mag does not imply that these are Miras (as opposed to SRVs). They are (candidate) LPVs and we do not distinguish between the two classes. The middle panel in Figure 5 shows considerable scatter between the amplitude in the I and K -band but also demonstrates that the majority of stars that have been classified as Miras based on I -band data have K -band amplitudes > 0.2 mag, in line with expectations.

In a subsequent step all known OGLE objects were removed, with the exception of those stars with periods longer than 1000 days as they are of prime interest here. This limit for a long period is arbitrary, but a limit of 1000 days was also used by Menzies et al. (2019) recently. Also stars detected by MACHO or EROS (and not by OGLE) were removed if the period listed by these surveys was in good agreement with the period found here (and not longer than 1000 days). Although these sources are not retained for further detailed analysis, the pulsation properties derived from the LC fitting are still available in Table A.3.

In a final step, the *Spitzer* IRS spectra of all those stars having a classification in the literature not being that of an O- or C-rich AGB star (see Table A.1) were inspected visually using the CASSIS tool⁵ (Combined Atlas of Sources with *Spitzer* IRS spectra, Lebouteiller et al. 2011). All spectra appeared consistent with the literature classification, and thus unlike those of O- or C-rich AGB stars. Therefore, they were removed from the sample of candidate LPVs. The exception is SMP LMC 11 (72.907608 – 67.088019). Although it is classified as a planetary nebula (PN) in SIMBAD, and the literature classification of its *Spitzer* IRS spectrum is that of a C-rich post-AGB star, its spectrum is, technically speaking, consistent with that of a very red C-rich AGB star and it is thus retained. At this point the sample of stars that will be investigated further is reduced to 254.

4.2. Creating and fitting the spectral energy distributions

As a further step in distinguishing AGB stars from non-AGB stars the SEDs of the 254 selected stars are constructed and fitted

⁵ <https://cassis.sirtf.com/>

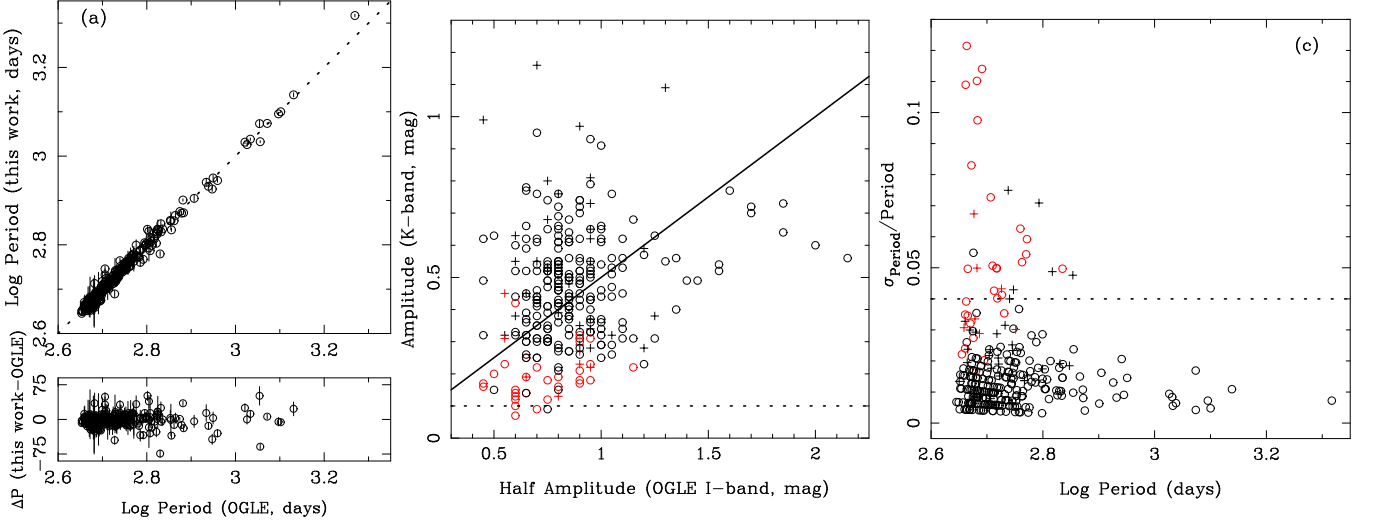


Fig. 5. Comparison between the pulsation properties of 294 confirmed Miras by OGLE with the results in the present work. The left panel (a) compares in the upper part the periods directly, with the dotted line marking the one-to-one relation. The lower part indicates the difference in periods as a function of the period found by OGLE. The star at $P = 1858$ d ($\log P = 3.26$) in the top panel is located outside the plot at $\Delta\text{Period} = 216$ d in the bottom panel. The middle panel (b) compares the amplitude in the K -band to that in the I -band. Note that the OGLE team defines amplitude as the minimum-to-maximum variation while we use the traditional definition (see Eq. 1). Stars with a $\chi^2_r > 430$ are marked by a plus sign, stars where the error on the K -band amplitude is larger than the amplitude are marked in red. The dotted line indicates the cut-off value of 0.1 mag used to select the maximum number of known Miras from our sample. The solid line has a slope 0.5 to guide the eye. The right hand panel (c) plots the relative error of the period determination against the period. Stars with a $\chi^2_r > 430$ are marked by a plus sign, stars where the error on the K -band amplitude is larger than the amplitude are marked in red. The dotted line indicates the cut-off value of 4% error on the period determination used to select Miras from our sample.

to a large sample of synthetic template SEDs of AGB stars and some non-AGB stars (created from some of the non-AGB stars previously discarded that have MIR spectra).

The procedure is largely outlined in GS18. Photometry is collected from AllWISE, SAGE, Akari, IRAS, OGLE and GDR2. In the NIR we use the mean K -band magnitude derived from the LC fitting. The VMC Y and J magnitude were downloaded from the VSA. The K_s -band listed in the VSA was also downloaded and assigned a large uncertainty of 0.1 mag so as to give this point less weight in the template fitting. As mentioned in Sect. 2.4.2, for some of the brightest stars the VMC photometry is influenced by non-linearity or saturation. For the SEDs the corresponding data points are plotted with large error bars (arbitrarily set at 0.25 mag) to identify them immediately and in order not to affect the fitting procedure. In some cases also the Y and J magnitudes may be affected by saturation as well and these are also assigned large error bars.

The magnitudes are then fitted to the synthetic photometry of several hundred templates. This indicates, with high reliability, whether the SED of a star is consistent with that of an O-rich, C-rich, or young stellar object (YSO) or other non-AGB objects. Details are given in Appendix C. The SEDs of all 254 objects with their best matching template are plotted in Fig. C.2.

Based on all available information (spectral type, MIR spectral classification, and template fitting) the 254 stars are divided into 217 most likely AGB stars, and 37 most likely non-AGB stars; see Table C.2. The latter group is no longer discussed, although it contains sources with variability properties that have similarities to those of LPVs. Figure 6 shows the light curves of a YSO and a B1 emission-line star as examples. Table A.1 lists a total of about 200 sources that have been associated with YSOs. An analysis of the VMC-based IR LCs of Spitzer-identified massive YSOs in a ~ 1.5 deg² area in the LMC will be presented in Zivkov et al. (2020).

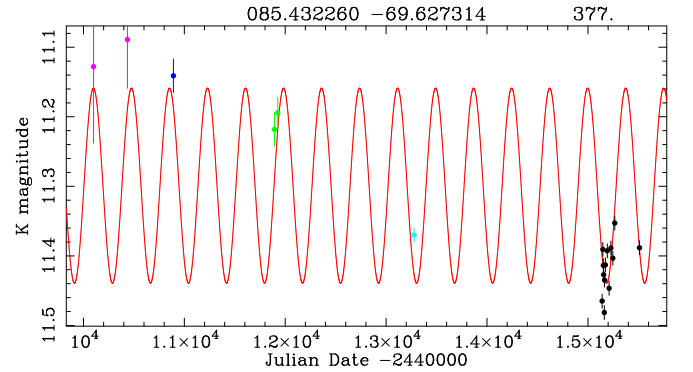


Fig. 6. Examples of LCs of objects where the literature classification and the template fitting point to a non-AGB nature. In the top panel the probable YSO object 2MASS J04573274 – 6959032 (based on a photometric classification; Table 10 in Gruendl & Chu 2009) and in the bottom panel the B1 emission-line star [BE74] 621. Data points (with error bars) are identified as follows: black: VMC, green: 2MASS, dark blue: 2MASS-6X, light blue: IRSF.

The classification based on the SED fitting is compared with that introduced by Lebzelter et al. (2018) for those AGB candidates for which the *Gaia* DR2 photometry is available (73 stars), as shown in Fig. 7. In Lebzelter et al. (2018) the division between O- and C-rich stars is performed according to their position on a specific diagram involving the difference between two Wesenheit functions obtained by combining the J , K_s , G_{BP} and G_{RP} photometric bands, $W_{RP,BP-RP} - W_{K_s,J-K_s}$ (see the left panel of Figure 1, and Table A.1 of Lebzelter et al. 2018). The Wesenheit functions are defined as:

$$W_{K_s,J-K_s} = K_s - 0.686 \cdot (J - K_s), \quad (2)$$

where J and K_s are the VISTA bands, and:

$$W_{RP,BP-RP} = WRP = G_{RP} - 1.3 \cdot (G_{BP} - G_{RP}). \quad (3)$$

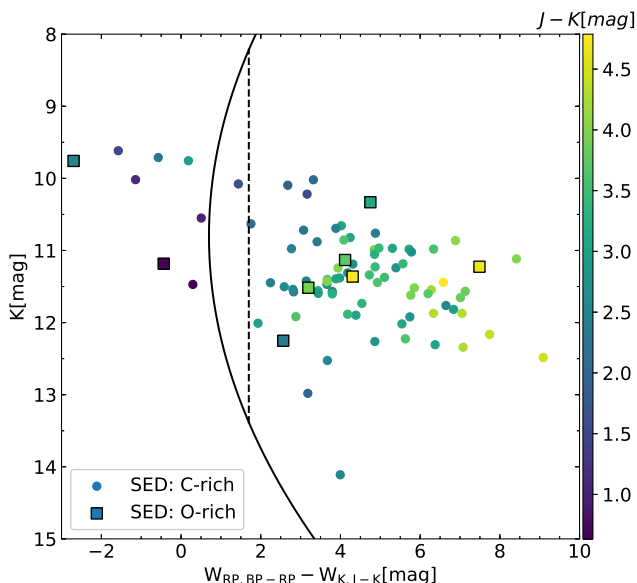


Fig. 7. Classification of the AGB candidates in this work based on the VISTA K_s -band and *GAIA* DR2 photometry (Lebzelter et al. 2018). The solid line indicates the separation between O-stars (to the left of the curve) and C-stars, while the dashed line separates C-stars from the most extreme dust enshrouded stars. All the stars are colour-coded according to their $(J - K)$ colours.

Among the selected stars, 65 sources are classified as C-rich and eight as O-rich. We find that 72 sources are classified as C-stars by both methods, while only six sources classified as extreme stars by Lebzelter et al. (2018) are classified as O-rich by the SED template fitting developed here. Two stars out of eight that are O-rich for Lebzelter et al. (2018) are classified as O-rich on the basis of the templates. Therefore, when considering the classification by Lebzelter et al. (2018), the SED classification method yields a comparable result for C-stars, but disagree on O-rich stars. According with the SED fitting classification method, among the 217 AGB candidates, 22 are O-rich, 1 is a PN and the remaining are C-rich stars.

The AGB candidates are also fitted using the public database of synthetic spectra and photometry for C-stars presented in Nanni et al. (2019). Such spectra are obtained by consistently computing the growth of dust grains of different species (amorphous carbon and silicon carbide for C-stars) coupled with a stationary dust-driven wind (Nanni et al. 2013, 2014) and a dust radiative transfer code (Groenewegen 2012). The optical constants for amorphous carbon dust are selected to reproduce the photometry in the IR and in the *Gaia* bands (Nanni et al. 2016; Nanni 2019). We here adopt the data set of Hanner (1988) combined with small grains $< 0.04 \mu\text{m}$. The metallicity of the synthetic models is $Z = 0.004$ and 0.006 for the SMC and LMC, respectively. As in Nanni et al. (2019) we select only those models among the ones computed for which the outflow is accelerated through dust-driven wind when the input MLR is $\log(\dot{M}) \geq -5.5 \text{ M}_{\odot} \text{ yr}^{-1}$. The best fit between the observed and synthetic photometry allows us to estimate the (gas) MLR, the dust production rate and the luminosity of each star, without the need to assume quantities such as the gas-to-dust ratio and the wind speed of the outflow. The results for the luminosity and MLRs derived from the fitting procedure are provided in Table D.1. In Fig. 8 the MLRs derived in this work and from Nanni et al. (2019) for sources in common are compared. We find that the results are in good agreement with a scatter of 0.23 dex.

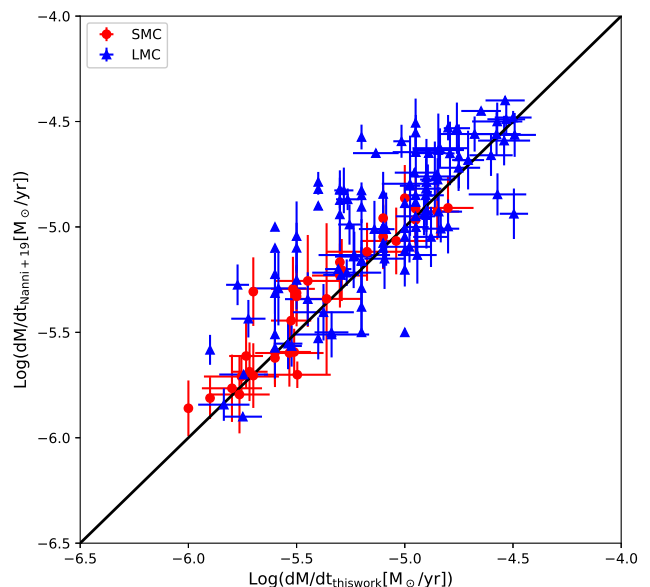


Fig. 8. Comparison between the MLR obtained by Nanni et al. (2019) against that derived in this work for stars in common. The solid black line is the one-to-one relation.

Only 44 and eight C-stars analysed in this work are missing from the analysis of Nanni et al. (2019) for the LMC and the SMC, respectively. Indeed, these sources were not included in the catalogues matched by Nanni et al. (2019) (which included C-stars from (Riebel et al. 2012; Ruffle et al. 2015; Srinivasan et al. 2016; Jones et al. 2017, GS18)). The total dust production rate of these missing stars is calculated, and it is found that their total contribution is negligible with respect to the total dust production rate of the entire AGB population in these galaxies.

The properties derived for the sources analysed in this work (period, bolometric luminosity and MLRs) are compared with those derived by Nanni et al. (2019) for the entire population of C-stars in the LMC for which the period has been determined (Riebel et al. 2012). The results are shown in Fig. 9, where we correlate the luminosity with the period, the MLR with the luminosity, and the MLR with the period. The sources analysed in this work span the entire range of M_{bol} while the periods are usually between $2.4 < \log P \text{ (d)} < 3.1$. The estimated MLR is in general greater than $\approx 10^{-6} \text{ M}_{\odot} \text{ yr}^{-1}$ and correlates with the luminosity, even though the scatter is large, and with the period.

5. Discussion

5.1. A comparison with periods from *Gaia*

Table 1 contains 32 sources which are listed in GDR2 with a ‘MIRA_SR’ classification and a period. The comparison with the period derived from the NIR data in the present paper is excellent; the value of $(P_{\text{Gaia}} - P_{\text{NIR}})/\sigma_{\text{Gaia}}$ ranges from -2.2 to $+2.4$ with a median value of $+0.1$. The periods that are presented here are more precise (the median error in the period is 70 days in the *Gaia* data and eight days in the present work), but the error in the period determination by *Gaia* is expected to decrease significantly with further data releases.

5.2. A comparison to the IRSF monitoring data in the SMC

Three stars in our sample have NIR monitoring data recently published by Ita et al. (2018) using the InfraRed Survey Facility

Table 1. Comparison of periods for sources in common between our study and *Gaia* DR2.

RA (deg)	Dec (deg)	GDR2 Source Id	Period <i>Gaia</i> (d)	Period this work (d)
04.876441	-72.465755	4689594530461666432	335 ± 29	265 ± 1
07.572240	-72.472302	4689184000304539520	531 ± 85	508 ± 12
08.511784	-72.363404	4689188428414841216	336 ± 37	356 ± 1
09.660904	-72.008445	4689221379397747968	513 ± 90	385 ± 8
09.828878	-70.131865	4702368897059777792	343 ± 27	320 ± 4
13.053875	-73.148050	4685938821845281280	821 ± 284	796 ± 5
13.292230	-72.198509	4689061778454380416	624 ± 157	491 ± 56
21.130633	-71.620707	4687594377067361280	549 ± 103	724 ± 12
25.642854	-71.369942	4687832356908117120	562 ± 172	545 ± 23
69.714864	-68.402870	4656274857070901760	580 ± 103	513 ± 2
73.110342	-68.577069	4655516060931435008	3937 ± 3845	744 ± 8
73.927019	-68.281715	4661533550631677184	466 ± 62	468 ± 7
74.358023	-74.020732	4649773380396677376	437 ± 50	547 ± 11
74.535830	-67.878353	4661558083486627328	433 ± 53	474 ± 13
74.536373	-71.966533	4654485474923219968	443 ± 73	536 ± 3
74.731098	-68.218399	4661543033920475392	612 ± 70	495 ± 10
76.076144	-74.117919	4649713079054327424	450 ± 58	493 ± 13
77.550727	-65.326051	4663596882956831104	664 ± 68	599 ± 98
78.161438	-64.203811	4664123102346900864	723 ± 216	883 ± 14
79.026012	-70.825900	4651988037356793600	515 ± 122	516 ± 10
79.994330	-70.471053	4651927113213190272	512 ± 56	455 ± 8
80.792265	-67.835106	4658834421384702208	593 ± 95	714 ± 34
80.802424	-64.158664	4661168096128809216	435 ± 43	449 ± 3
81.285698	-73.278491	4651133854242537728	321 ± 25	310 ± 6
82.281667	-66.970853	4660210735084020608	495 ± 54	490 ± 6
82.751418	-69.179865	4658428873394148352	645 ± 174	612 ± 32
83.558539	-68.978837	4658446499944028800	550 ± 249	548 ± 7
83.720398	-71.006350	4657091970360446464	710 ± 121	715 ± 7
83.767073	-69.954142	4657247619989849472	532 ± 61	523 ± 21
85.201902	-69.560027	4657599188763136896	1173 ± 829	576 ± 5
86.488037	-64.462946	4756251319078635648	423 ± 55	388 ± 9
89.223262	-67.070124	4659600643536501504	509 ± 87	414 ± 35

Notes. GDR2 does not list periods but a frequency ω and its error σ . Period and error are calculated as $1/\omega$ and $1/\omega - 1/(\omega + \sigma)$ for simplicity.

(IRSF, Kato et al. 2007). These data were not used in our LC analysis, and can therefore serve as an independent test. The *K*-band data (*H*-band for 12.627600 – 72.858307) were analysed in the same way as the VMC data complemented with literature data. Table 2 compares the periods and amplitudes. For the first two stars the agreement is good. In the last case the periods do not agree within their mutual error bars, but this is a faint source for the IRSF survey ($K \sim 15.5$ mag) while our analysis might be hampered by the relatively small number of data points (18 in total).

5.3. LPVs with periods over 1000 days

Among the likely AGB stars 34 stars have periods longer than 1000 days⁶. The longest period we find is 3108 d, but this object has alternative periods that are much shorter. Six other stars also have shorter possible periods, and therefore the periods beyond 1000 days are only tentative in these cases. It will be interesting to analyse the IRSF data for the LMC objects when it becomes available (cf. the SMC data presented in Ita et al. 2018).

Nine stars with periods over 1000 days in the MCs were previously reported by Wood et al. (1992) and Whitelock et al. (2003) based on NIR observations. Recently, Menzies et al.

(2019) presented a compilation of Miras with periods over 1000 days in the Milky Way (17), SMC (3), and LMC (18), while Karambelkar et al. (2019) published a list of 417 luminous infrared variables, of which 86 have periods over 1000 days, located in seven galaxies (the majority in M 83 (49 objects), and M 81 (11 objects)). The compilation by Menzies et al. (2019) was based on Wood et al. (1992) and Whitelock et al. (2003), OGLE data in the SMC and LMC (Soszyński et al. 2011, 2009a), and GS18 (which is partly based on a preliminary analysis of VMC data). Of the 21 MC objects, 18 are confirmed with updated periods. Three objects are not in our list. One object (IRAS 05506–7053) is too red; the period in GS18 is based on *WISE* data. The two others (HV 888 and HV 11417) are too blue to have passed the selection criteria, and both have been classified as RSGs (GS18, Kraemer et al. 2017).

The longest period in the study of GS18 of almost 400 AGB stars with *Spitzer* IRS spectra is 1810 d based on a re-analysis of OGLE-III data for MSX SMC 055 (OGLE-SMC-LPV-08137, IRAS 00483 – 7347). No error on the period is given in GS18 as they are very hard to reliably estimate for these long periods. The period in the OGLE-III release is 1859 d which gives some indication of the uncertainty. In Groenewegen et al. (2009) such a long-period was already recognised based on OGLE-II data and it was suggested that the object may be a candidate super-AGB star, based on its long period and very high luminosity. Updated

⁶ We include one star with a period of 997 ± 12 days.

Table 2. Comparison with three sources in the IRSF survey.

RA (deg)	Dec (deg)	Filter	Period (d)	Amplitude (mag)	Period (d)	Amplitude (mag)
			IRSF		VMC	
12.627600	-72.858307	<i>H</i>	1035.8 ± 5.3	0.39 ± 0.04	1062 ± 10	0.56 ± 0.05 ^a
14.860309	-72.394926	<i>K</i>	421.9 ± 1.0	0.54 ± 0.03	434 ± 3	0.52 ± 0.20
15.173292	-72.633497	<i>K</i>	391.6 ± 2.4	0.53 ± 0.14	451 ± 7	0.37 ± 0.15

Notes. ^(a) In the *K*-band.

parameters were given in GS18, where a current pulsation mass of about 9 M_{\odot} was derived. It has a large amplitude (0.8 mag in *I*) but its LC is not very regular in shape (see the middle panel of Fig. 7 in Soszyński et al. 2011). Based on the IR LC a period of 2075 ± 15 d is derived here, about 4 σ away from the optically determined period considering the mutual error bars.

There are two stars in the present sample of likely AGB stars that have very long periods⁷. They are VMC J052454.84 – 682958.02 (81.228480 – 68.499449) with $P = 2261 \pm 41$ d and amplitude 0.20 ± 0.02 mag, and VMC J045211.18 – 701244.83 (73.046582 – 70.212454) with $P = 2510 \pm 67$ d and amplitude 0.15 ± 0.06 mag. Little is known about the former source. It is not listed in SIMBAD. Its SED is very well fitted by that of a dusty O-rich star, but its luminosity based on the template fitting is low ($L \sim 1500 L_{\odot}$), and its amplitude small for a Mira variable. The latter source is listed as a candidate post-AGB object. In ViZier there are catalogues associated with a source classified as a PN, but often located at about 2'' away. VMC *Y* and *K_s*-band images were inspected. The finding chart in Morgan (1994) (object 9) suffers from poor resolution and is not clear. A slightly better chart was published by Leisy et al. (1997) but it does not allow to unequivocally distinguish between two sources in the VMC images. The coordinates published there and in Reid & Parker (2006) (RP 1607) refer to a source located at about 2.2'' to the SE of the very red VMC source referred to in this paper. In any case, the luminosity based on the template fitting is low ($L \sim 3000 L_{\odot}$), and its amplitude small for a Mira variable.

One of the original ideas behind this work was to find stars with very long periods as a tracer of the most massive AGB and super-AGB stars. The nature of the two stars with 2000+ day periods would be interesting to investigate but they are unlikely to be as massive as the about 9 M_{\odot} estimated for MSX SMC 055 (GS18).

5.4. The bolometric PL-relation

Figure 10 shows the bolometric *PL*-relation. The top panel shows all 254 objects for which the template fitting was performed. The likely C-rich objects (i.e. listed as ‘C’ in col. 10 in Table C.2) are plotted as open squares, the likely O-rich objects (i.e. listed as ‘O’ in Table C.2) are plotted as open triangles, the other AGB stars (i.e. listed as O(AGB), O(OTH), C(AGB) in Table C.2) as filled circles. The 37 likely non-AGB stars are plotted as dots. The likely C-rich Miras (with an amplitude > 0.2 mag) are plotted in the middle panel. The blue dashed line is a fit to the data, excluding seven outliers (plotted as dots) based on iterative 3 σ clipping. The fit is $M_{\text{bol}} =$

$(-2.27 \pm 0.20) \cdot \log P + (1.45 \pm 0.54)$ mag using 182 stars and with an rms of 0.41 mag using a linear bi-sector fit (using the code SIXLIN from Isobe et al. 1990). Restricting the sample to LMC objects only (144 objects), or eliminating the objects for which an alternative period can not be excluded, do not significantly change the coefficients of the fit or the rms value.

The likely O-rich Miras (with an amplitude > 0.2 mag) are plotted in the bottom panel. The blue dashed line is a fit to the data, excluding two outliers (plotted as dots) based on iterative 3 σ clipping. The fit is $M_{\text{bol}} = (-2.97 \pm 0.09) \cdot \log P + (2.59 \pm 0.28)$ mag based on 11 stars and with an rms of 0.36 mag. The red dotted lines in the two panels indicate relations from Feast et al. (1989) for C- and O-rich Miras in the LMC respectively. These relations were derived for $P < 420$ d, and were shifted using an LMC distance modulus of 18.477 mag from Pietrzyński et al. (2019).

6. Summary

Based on CCD and CMD diagrams and the properties of known Mira variables detected by the OGLE survey a sample of 1299 sources is selected as (candidate) LPVs with periods longer than 450 days. Multiple VMC *K_s*-band data are combined with literature data to construct LCs. A limitation is that magnitudes from different *K*-type filters are mixed, as it is close to impossible to uniformly and consistently convert all data to a uniform system. The LCs are analysed for periodic variations. Mean magnitudes are published for all stars, and periods and amplitudes for 949 stars. Based on the pulsation properties of known OGLE Miras, and removing all stars with a known period (except when longer than 1000 days), a sample of 254 stars is retained for further study. The spectral energy distributions of these stars are derived and fitted with template distributions of known objects. A final list of 217 candidate LPVs is obtained. Thirty-four objects have periods longer than 1000 days, but some have a viable alternative period that is shorter. The longest-period known Mira in the Magellanic Clouds from OGLE data (with $P = 1810$ d) is derived to have a period of 2075 d based on its IR LC. Two stars are found to have longer periods, but both have luminosities and pulsation amplitudes unlike those of Miras. The bolometric magnitude - period relation is derived for both likely O- and C-rich stars in the sample.

Acknowledgements. We thank the Cambridge Astronomy Survey Unit (CASU) and the Wide Field Astronomy Unit (WFAU) in Edinburgh for providing calibrated data products under the support of the Science and Technology Facility Council (STFC) in the UK. M.-R.L.C acknowledges support from the European Research Council (ERC) under the European Union’s Horizon 2020 research and innovation programme (grant agreement No 682115). A.N. acknowledges support from the Centre National d’Etudes Spatiales (CNES) through a post-doctoral fellowship. This publication is partly based on the OGLE observations obtained with the Warsaw Telescope at the Las Campanas Observatory, Chile, operated by the Carnegie Institution of Washington. This paper utilises public domain data originally obtained by the MACHO Project, whose work was performed under the joint auspices of the U.S. Department of Energy, National Nuclear

⁷ Excluding 70.632433 – 74.796568 with $P = 3108$ d because of the possible presence of also a shorter period, and 81.098476 – 65.536337 with $P = 2125$ d but a rather poor fit and an uncertain amplitude of 0.38 ± 0.18 mag.

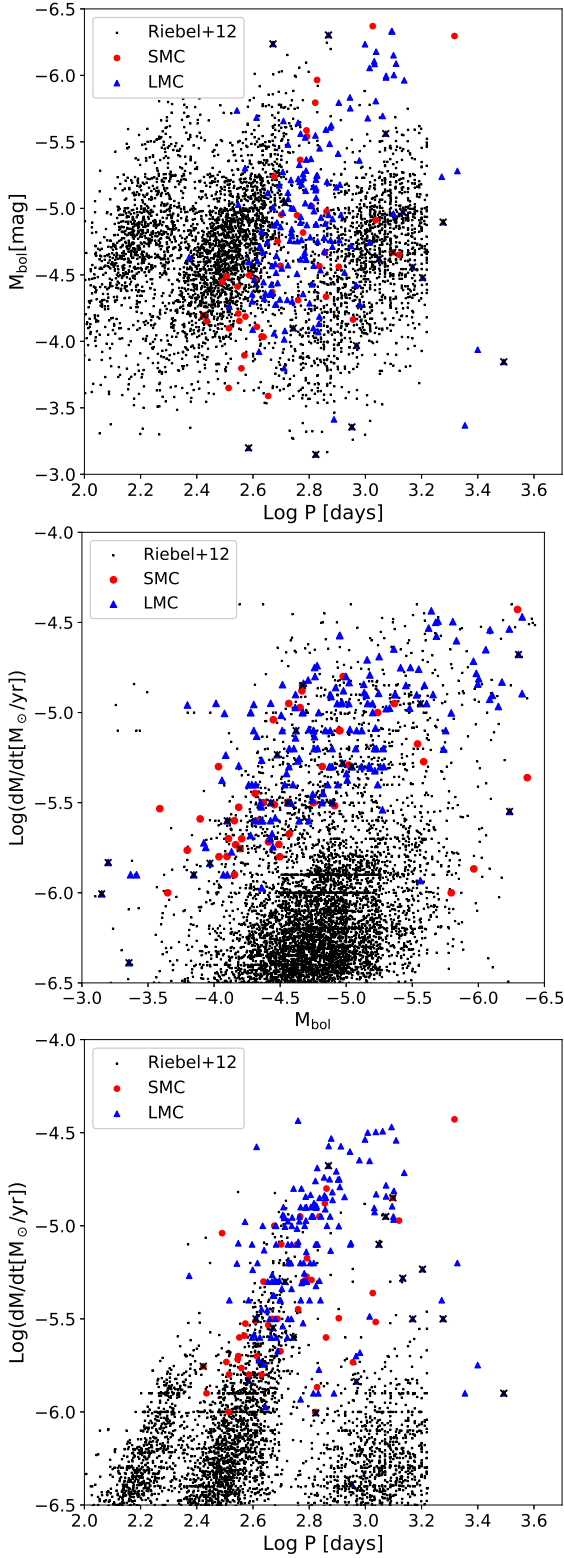


Fig. 9. Top panel: bolometric luminosity versus period obtained from the SED fitting of the C-stars selected in this work: C-stars in the SMC are indicated with red dots, while C-stars in the LMC are plotted with blue triangles. For comparison, we over plot the population of C-stars in the LMC for which the period has been determined from Riebel et al. (2012) which have been fitted by Nanni et al. (2019). To avoid superposition in the plot, M_{bol} has been changed by a random number between -0.25 and $+0.25$ mag. The sources for which the period has been flagged with a superscript ‘a’ or ‘b’ in Table C.2 have been indicate with a cross. The middle and bottom panels show the relations between MLR versus the bolometric luminosity and MLR versus period, respectively.

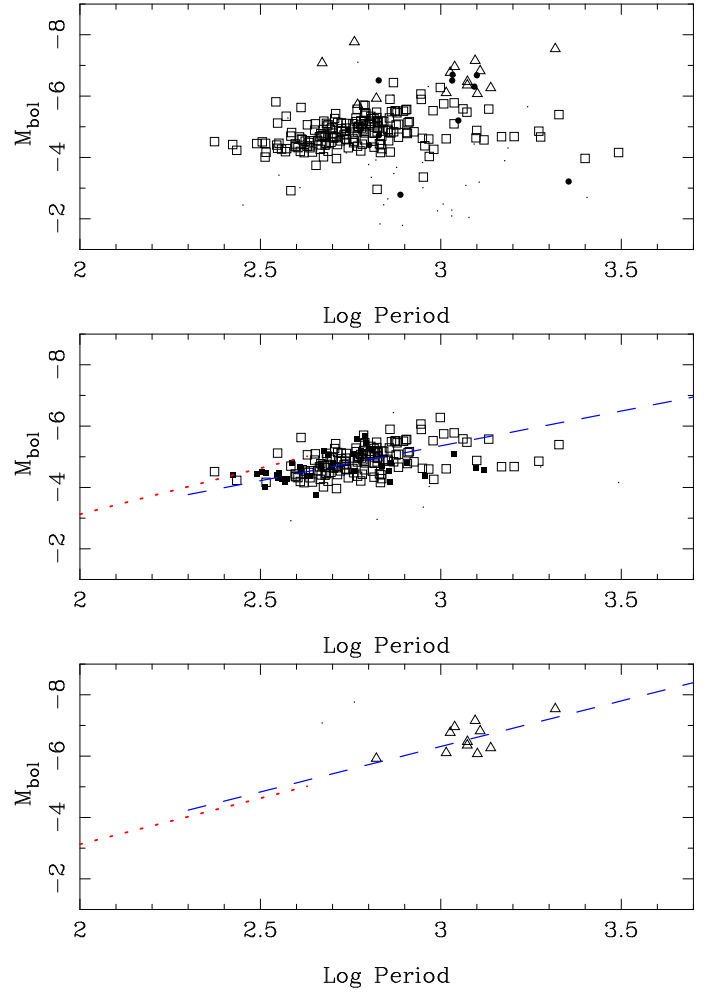


Fig. 10. Bolometric PL -relations for all the 254 objects for which the template fitting was performed (top panel), and the subsets of likely C-rich Miras (middle panel), and O-rich Miras (bottom panel). The likely C-rich objects are plotted as open squares, the likely O-rich objects are plotted as open triangles, the other AGB stars as filled circles, see the main text for details. The 37 likely non-AGB stars are plotted as dots. The likely C-rich Miras (with an amplitude > 0.2 mag) are plotted in the middle panel. The objects in the LMC are plotted with open symbols, those in the SMC with filled symbols. The blue dashed line is a fit to the data, excluding outliers (plotted as dots). The likely O-rich Miras (with an amplitude > 0.2 mag) are plotted in the bottom panel. The blue dashed line is a fit to the data, excluding outliers (plotted as dots). The red dotted lines in the two panels indicate relations from the literature derived at shorter periods, see the main text for details.

Security Administration by the University of California, Lawrence Livermore National Laboratory under contract No. W-7405-Eng-48, the National Science Foundation through the Center for Particle Astrophysics of the University of California under cooperative agreement AST-8809616, and the Mount Stromlo and Siding Spring Observatory, part of the Australian National University. This publication makes use of data products from the Wide-field Infrared Survey Explorer, which is a joint project of the University of California, Los Angeles, and the Jet Propulsion Laboratory/California Institute of Technology, funded by the National Aeronautics and Space Administration. This research has made use of the SIMBAD database and the VizieR catalogue access tool, both operated at CDS, Strasbourg, France. This work has made use of data from the European Space Agency (ESA) mission *Gaia* (<https://www.cosmos.esa.int/gaia>), processed by the *Gaia* Data Processing and Analysis Consortium (DPAC, <https://www.cosmos.esa.int/web/gaia/dpac/consortium>). Funding for the DPAC has been provided by national institutions, in particular the institutions participating in the *Gaia* Multilateral Agreement.

References

- Aringer, B., Girardi, L., Nowotny, W., Marigo, P., & Lederer, M. T. 2009, *A&A*, 503, 913
- Aringer, B., Marigo, P., Nowotny, W., et al. 2019, *MNRAS*, 487, 2133
- Bessell, M. S. & Brett, J. M. 1989, *JHKLM Photometry: Standard Systems, Passbands and Intrinsic Colors*, ed. E. F. Milone, Vol. 341, 61
- Bolatto, A. D., Simon, J. D., Stanimirović, S., et al. 2007, *ApJ*, 655, 212
- Boyer, M. L., Srinivasan, S., van Loon, J. T., et al. 2011, *AJ*, 142, 103
- Carpenter, J. M. 2001, *AJ*, 121, 2851
- Cioni, M.-R. L., Clementini, G., Girardi, L., et al. 2011, *A&A*, 527, A116
- Cioni, M.-R. L., Ripepi, V., Clementini, G., et al. 2017, in *European Physical Journal Web of Conferences*, Vol. 152, European Physical Journal Web of Conferences, 01008
- Cross, N. J. G., Collins, R. S., Mann, R. G., et al. 2012, *A&A*, 548, A119
- Cutri, R. M., Skrutskie, M. F., van Dyk, S., et al. 2003, *VizieR Online Data Catalog*, II/246
- Cutri, R. M., Skrutskie, M. F., van Dyk, S., et al. 2012, *VizieR Online Data Catalog*, II/281
- Cutri, R. M., Wright, E. L., Conrow, T., et al. 2013, *VizieR Online Data Catalog*, 2328, 0
- DENIS Consortium. 2005, *VizieR Online Data Catalog*, 2263
- Emerson, J. & Sutherland, W. 2010, *The Messenger*, 139, 2
- Feast, M. W., Glass, I. S., Whitelock, P. A., & Catchpole, R. M. 1989, *MNRAS*, 241, 375
- Ferraro, F. R., Fusi Pecci, F., Testa, V., et al. 1995, *MNRAS*, 272, 391
- Fraser, O. J., Hawley, S. L., & Cook, K. H. 2008, *AJ*, 136, 1242
- Frogel, J. A., Mould, J., & Blanco, V. M. 1990, *ApJ*, 352, 96
- Gaia Collaboration, Brown, A. G. A., Vallenari, A., et al. 2018, *A&A*, 616, A1
- Glass, I. S. & Evans, T. L. 1981, *Nature*, 291, 303
- Glass, I. S. & Reid, N. 1985, *MNRAS*, 214, 405
- Gordon, K. D., Meixner, M., Meade, M. R., et al. 2011, *AJ*, 142, 102
- Groenewegen, M. A. T. 2004, *A&A*, 425, 595
- Groenewegen, M. A. T. 2012, *A&A*, 543, A36
- Groenewegen, M. A. T. & Blommaert, J. A. D. L. 1998, *A&A*, 332, 25
- Groenewegen, M. A. T., Sevenster, M., Spoon, H. W. W., & Pérez, I. 2002, *A&A*, 390, 511
- Groenewegen, M. A. T. & Sloan, G. C. 2018, *A&A*, 609, A114
- Groenewegen, M. A. T., Sloan, G. C., Soszyński, I., & Petersen, E. A. 2009, *A&A*, 506, 1277
- Groenewegen, M. A. T., Vlemmings, W. H. T., Marigo, P., et al. 2016, *A&A*, 596, A50
- Gruendl, R. A. & Chu, Y.-H. 2009, *ApJS*, 184, 172
- Gullieuszik, M., Groenewegen, M. A. T., Cioni, M.-R. L., et al. 2012, *A&A*, 537, A105
- Hanner, M. 1988, *Grain optical properties*, Tech. rep.
- Hauschildt, P. H., Allard, F., & Baron, E. 1999, *ApJ*, 512, 377
- Höfner, S. & Olofsson, H. 2018, *A&A Rev.*, 26, 1
- Holl, B., Audard, M., Nienartowicz, K., et al. 2018, *A&A*, 618, A30
- Houck, J. R., Roellig, T. L., van Cleve, J., et al. 2004, *ApJS*, 154, 18
- Huang, C. D., Riess, A. G., Hoffmann, S. L., et al. 2018, *ApJ*, 857, 67
- Huang, C. D., Riess, A. G., Yuan, W., et al. 2020, *ApJ*, 889, 5
- Hughes, S. M. G. 1989, *AJ*, 97, 1634
- Hughes, S. M. G. & Wood, P. R. 1990, *AJ*, 99, 784
- Irwin, M. J. 2009, *UKIRT Newsletter*, 25, 15
- Isobe, T., Feigelson, E. D., Akritas, M. G., & Babu, G. J. 1990, *ApJ*, 364, 104
- Ita, Y., Matsunaga, N., Tanabé, T., et al. 2018, *MNRAS*, 481, 4206
- Ita, Y., Tanabé, T., Matsunaga, N., et al. 2004, *MNRAS*, 347, 720
- Ivezić, Ž., Nenkova, M., & Elitzur, M. 1999, *DUSTY: Radiation transport in a dusty environment*, Astrophysics Source Code Library
- Jones, O. C., Woods, P. M., Kemper, F., et al. 2017, *MNRAS*, 470, 3250
- Kamath, D., Wood, P. R., Soszyński, I., & Lebzelter, T. 2010, *MNRAS*, 408, 522
- Karambelkar, V. R., Adams, S. M., Whitelock, P. A., et al. 2019, *ApJ*, 877, 110
- Kastner, J. H., Thorndike, S. L., Romanczyk, P. A., et al. 2008, *AJ*, 136, 1221
- Kato, D., Nagashima, C., Nagayama, T., et al. 2007, *PASJ*, 59, 615
- Kim, D.-W., Protopapas, P., Bailer-Jones, C. A. L., et al. 2014, *A&A*, 566, A43
- Koen, C., Marang, F., Kilkeny, D., & Jacobs, C. 2007, *MNRAS*, 380, 1433
- Kraemer, K. E., Sloan, G. C., Wood, P. R., Jones, O. C., & Egan, M. P. 2017, *ApJ*, 834, 185
- Lebouteiller, V., Barry, D. J., Spoon, H. W. W., et al. 2011, *ApJS*, 196, 8
- Lebzelter, T., Mowlavi, N., Marigo, P., et al. 2018, *A&A*, 616, L13
- Leisy, P., Dennefeld, M., Alard, C., & Guibert, J. 1997, *A&AS*, 121, 407
- Lenz, P. & Breger, M. 2005, *Communications in Asteroseismology*, 146, 53
- Meixner, M., Gordon, K. D., Indebetouw, R., et al. 2006, *AJ*, 132, 2268
- Menzies, J. W., Whitelock, P. A., Feast, M. W., & Matsunaga, N. 2019, *MNRAS*, 483, 5150
- Morgan, D. H. 1994, *A&AS*, 103, 235
- Muraveva, T., Subramanian, S., Clementini, G., et al. 2018, *MNRAS*, 473, 3131
- Nanni, A. 2019, *MNRAS*, 482, 4726
- Nanni, A., Bressan, A., Marigo, P., & Girardi, L. 2013, *MNRAS*, 434, 2390
- Nanni, A., Bressan, A., Marigo, P., & Girardi, L. 2014, *MNRAS*, 438, 2328
- Nanni, A., Groenewegen, M. A. T., Aringer, B., et al. 2019, *MNRAS*, 487, 502
- Nanni, A., Marigo, P., Girardi, L., et al. 2018, *MNRAS*, 473, 5492
- Nanni, A., Marigo, P., Groenewegen, M. A. T., et al. 2016, *MNRAS*, 462, 1215
- Nishida, S., Tanabé, T., Nakada, Y., et al. 2000, *MNRAS*, 313, 136
- Oliveira, J. M., van Loon, J. T., Chen, C. H. R., et al. 2009, *ApJ*, 707, 1269
- Payne-Gaposchkin, C. H. 1971, *Smithsonian Contributions to Astrophysics*, 13
- Pietrzyński, G., Graczyk, D., Gallenne, A., et al. 2019, *Nature*, 567, 200
- Pojmanski, G. 2002, *Acta Astron.*, 52, 397
- Press, W. H., Teukolsky, S. A., Vetterling, W. T., & Flannery, B. P. 1992, *Numerical recipes in FORTRAN. The art of scientific computing*
- Ramstedt, S. & Olofsson, H. 2014, *A&A*, 566, A145
- Reid, I. N., Hughes, S. M. G., & Glass, I. S. 1995, *MNRAS*, 275, 331
- Reid, N. 1991, *ApJ*, 382, 143
- Reid, N., Tinney, C., & Mould, J. 1990, *ApJ*, 348, 98
- Reid, W. A. 2014, *MNRAS*, 438, 2642
- Reid, W. A. & Parker, Q. A. 2006, *MNRAS*, 373, 521
- Riebel, D., Srinivasan, S., Sargent, B., & Meixner, M. 2012, *ApJ*, 753, 71
- Ripepi, V., Cioni, M.-R. L., Moretti, M. I., et al. 2017, *MNRAS*, 472, 808
- Ripepi, V., Marconi, M., Moretti, M. I., et al. 2016, *ApJS*, 224, 21
- Ripepi, V., Moretti, M. I., Marconi, M., et al. 2015, *MNRAS*, 446, 3034
- Ripepi, V., Moretti, M. I., Marconi, M., et al. 2012, *MNRAS*, 424, 1807
- Ruffle, P. M. E., Kemper, F., Jones, O. C., et al. 2015, *MNRAS*, 451, 3504
- Sanduleak, N., MacConnell, D. J., & Philip, A. G. D. 1978, *PASP*, 90, 621
- Seale, J. P., Looney, L. W., Chu, Y.-H., et al. 2009, *ApJ*, 699, 150
- Skiff, B. A. 2014, *VizieR Online Data Catalog*, 1
- Sloan, G. C., Kraemer, K. E., McDonald, I., et al. 2016, *ApJ*, 826, 44
- Soszyński, I., Dziembowski, W. A., Udalski, A., et al. 2007, *Acta Astron.*, 57, 201
- Soszyński, I., Poleski, R., Udalski, A., et al. 2008a, *Acta Astron.*, 58, 163
- Soszyński, I., Udalski, A., Poleski, R., et al. 2012, *Acta Astron.*, 62, 219
- Soszyński, I., Udalski, A., Szymański, M. K., et al. 2010, *Acta Astron.*, 60, 91
- Soszyński, I., Udalski, A., Szymański, M. K., et al. 2008b, *Acta Astron.*, 58, 293
- Soszyński, I., Udalski, A., Szymański, M. K., et al. 2009a, *Acta Astron.*, 59, 239
- Soszyński, I., Udalski, A., Szymański, M. K., et al. 2009b, *Acta Astron.*, 59, 335
- Soszyński, I., Udalski, A., Szymański, M. K., et al. 2011, *Acta Astron.*, 61, 217
- Spano, M., Mowlavi, N., Eyer, L., et al. 2011, *A&A*, 536, A60
- Srinivasan, S., Boyer, M. L., Kemper, F., et al. 2016, *MNRAS*, 457, 2814
- Tanabé, T., Nishida, S., Matsumoto, S., et al. 1997, *Nature*, 385, 509
- Trabucchi, M., Wood, P. R., Montalbán, J., et al. 2017, *ApJ*, 847, 139
- Ulaczyk, K., Szymański, M. K., Udalski, A., et al. 2013, *Acta Astron.*, 63, 159
- van Loon, J. T., Zijlstra, A. A., Whitelock, P. A., et al. 1997, *A&A*, 325, 585
- Westerlund, B. E. & Smith, L. F. 1964, *MNRAS*, 128, 311
- Whitelock, P. A., Feast, M. W., Menzies, J. W., & Catchpole, R. M. 1989, *MNRAS*, 238, 769
- Whitelock, P. A., Feast, M. W., van Loon, J. T., & Zijlstra, A. A. 2003, *MNRAS*, 342, 86
- Whitney, B. A., Sewilo, M., Indebetouw, R., et al. 2008, *AJ*, 136, 18
- Wood, P. R. 1998, *A&A*, 338, 592
- Wood, P. R. 2000, *PASA*, 17, 18
- Wood, P. R., Alcock, C., Allsman, R. A., et al. 1999, in *IAU Symposium*, Vol. 191, Asymptotic Giant Branch Stars, ed. T. Le Bertre, A. Lèbre, & C. Waelkens, 151
- Wood, P. R., Bessell, M. S., & Fox, M. W. 1983, *ApJ*, 272, 99
- Wood, P. R., Whiteoak, J. B., Hughes, S. M. G., et al. 1992, *ApJ*, 397, 552
- Woods, P. M., Oliveira, J. M., Kemper, F., et al. 2011, *MNRAS*, 411, 1597
- Zickgraf, F. J., Wolf, B., Stahl, O., & Humphreys, R. M. 1989, *A&A*, 220, 206
- Zickgraf, F. J., Wolf, B., Stahl, O., Leitherer, C., & Appenzeller, I. 1986, *A&A*, 163, 119
- Zijlstra, A. A., Loup, C., Waters, L. B. F. M., et al. 1996, *MNRAS*, 279, 32
- Zivkov, V., Oliveira, J. M., Petr-Gotzens, M. G., et al. 2020, *arXiv e-prints*, arXiv:2002.12291

Appendix A: The sample, literature and period analysis

Tables A.1, A.2 and A.3 provide the first entries of the tables available at the CDS. They provide information about the 1299 sources for which the K -band LCs were analysed. Table A.1 provides basic information about the sample, Table A.2 provides information on known periodicity from the literature, while Table A.3 provides the results of the LC analysis. The meaning of the columns is explained in the footnotes to the Tables.

Figure A.1 shows examples of the LC fitting. The complete set for the 1299 objects for which this was performed is available in the on-line edition. The model is represented by the (red) solid line. On top of the plot the identifier and the period (in days) are listed.

Appendix B: The effect of mixing different K -band filters in the analysis

No attempt was made to bring the various K -band measurements onto a common system. Various reasons (see Sect. 2.4.2) would make a colour transformation particularly complicated and uncertain in many cases. This is a limitation, and we try to estimate the possible effect now.

Examination of the bolometric corrections computed by Aringer et al. (2009, 2019), limited to the coolest of their spectra ($T_{\text{eff}} = 2600$ K), reveals that the expected magnitude differences between a K passband (from Bessell & Brett 1989) and a 2MASS K_s filter are typically smaller than 0.04 mag for O-rich stars, and smaller than 0.015 mag for C-rich stars. Such differences are smaller for stars with hotter photospheres.

We also investigated the synthetic photometry of the best fits to the SEDs and IRS spectra of almost 400 AGB and RSG stars (GS18) that span a very wide range in colour. We compared K -band magnitudes in the VISTA, DENIS, IRSF, 2MASS and SAAO systems. For stars with moderate circumstellar reddening ($J - K \lesssim 2$) the differences between VISTA and DENIS, and VISTA and 2MASS are of the order quoted above, i.e. $\lesssim 0.02$ mag. For redder stars, the differences are of order $0.03 - 0.04$ mag at $J - K = 5$. The effect in the IRSF filter is less, and in the SAAO system greater, up to 0.2 mag for the redder stars. It is noted that these colours are much redder than the transformation formula given in Koen et al. (2007) which are derived in the range $-0.087 \leq (J - K) \leq 1.390$.

The effect of a 0.2 mag change in the externally available photometry (independent of the filter system) is tested on eight stars monitored by Whitelock et al. (2003) without detection in the J -band, which, based on their $(H - K)$ colour, have an estimated $(J - K) \gtrsim 4$ mag. Their periods range from 550 to 1375 days and their amplitudes from 0.4 to 0.9 mag. The corresponding offset is applied to each of the stars considered, and the period analysis repeated. The absolute differences in the mean magnitudes are 0.01-0.07 mag, and this corresponds to, at most, a 1.2σ difference with respect to the quoted error bar (for six stars the difference is $< 0.5\sigma$). The absolute differences in periods are 1-8 days, and this corresponds to, at most, a 1.8σ difference with respect to the quoted error bar (for six stars the difference is $< 0.3\sigma$). The absolute differences in amplitudes are 0.01-0.06 mag, and this corresponds to, at most, a 1.3σ difference with respect to the quoted error bar (for five stars the difference is $< 0.3\sigma$).

We conclude therefore that the differences between different filter systems is in most cases smaller than the quoted error bars and do not influence the results of this paper.

Appendix C: Spectral energy distributions and template fitting

To obtain insights into the nature of the objects the SEDs are constructed and compared in a quantitative way to the synthetic SEDs of sources of known composition. For the AGB stars we use as templates the synthetic photometry of the best-fits to the SEDs and *Spitzer* spectra of O-rich AGB stars, RSGs, and C-rich AGB stars from GS18, respectively, 82, 76 and 204 objects. These stars cover a large range in effective temperatures, MLRs and dust compositions. The distinction made in GS18 between O-rich AGB stars and RSGs is based on a number of properties including luminosity and pulsation period following the discussion in Sect. 5.1 in Groenewegen et al. (2009).

From Table A.1 and the discussion in Sect. 4.1 it is clear that the main interlopers among possible LPVs on the AGB are YSOs, but also objects classified as HII regions, hot stars (Be stars or blue supergiants (BSG)), Wolf-Rayet (WR) stars or post-AGB/PN stars could be among the sample of 254 candidate LPVs. To have these types of sources represented among the templates a few sources were picked and analysed in detail, as outlined in the next section.

Appendix C.1: The fitting of some non-AGB templates

One PN, one Wolf-Rayet star, one HII region, three blue BSGs and six (candidate) YSOs with IRS spectra are selected for a detailed study from the objects in Table A.1. The exception is iras05216 (80.37° – 67.85°) that was initially considered by GS18 as an AGB star but eliminated in the process as its SED and IRS spectrum were not consistent with that of an AGB star. Information on these stars is provided in Table C.1.

Like in GS18 the SEDs and the *Spitzer* IRS spectra are fitted with More of DUSTY (MoD, Groenewegen 2012), an extension of the radiative transfer code DUSTY (Ivezić et al. 1999). For a given set of photometry and spectra as input data the programme determines the best fitting luminosity, dust optical depth, dust temperature at the inner radius, and slope of the density profile.

The stars are hotter than AGB stars and the PHOENIX model atmospheres (Hauschildt et al. 1999) are used to represent the central star⁸. The dust is a combination of amorphous silicates, corundum, and metallic iron, or amorphous carbon and silicon carbide similar to that in GS18. The proportions between the species are chosen as to reasonably fit the dust continuum and broad dust features of the *Spitzer* spectrum. The actual dust composition may be more complicated, but it is not our aim to study this in detail in this paper.

The fits are shown in Figure C.1. Overall the fits are reasonable representations of the photometric data and that is the main purpose of this exercise. The synthetic photometry corresponding to these fits can serve as representative templates.

There are also clear shortcomings, for example the spectra show the presence of polycyclic aromatic hydrocarbon and other features that are not included in the model. In addition DUSTY and MoD are one-dimensional codes while the geometry around the YSOs is often clearly non-spherical. For this reason the fit parameters are not discussed in detail as they are sometimes unphysical, such as dust temperatures at the inner radius above 2000 K.

⁸ <https://phoenix.ens-lyon.fr/Grids/BT-NextGen/SPECTRA/>

Table A.1. Sample for which a period analysis and LC fitting was performed.

RA (deg)	Dec (deg)	Names	Object Type	Spectral Type	Gaia Type	Spitzer Type
4.876441	-72.465755	2MASS J00193036-7227567	Can. AGB		MIRA_SR	
5.993721	-73.631895	OGLE SMC-LPV-190, 2MASS J00235849-7337548	Mira			
6.088240	-72.107443					
6.498306	-73.895774	OGLE SMC-LPV-367 2MASS J00255959-7353448	Mira			
6.795538	-73.408413	OGLE SMC-LPV-486 2MASS J00271093-7324303	Mira			
7.329711	-71.063852	IRAS F00271-7120 2MASS J00291916-7103499	C	C		
7.572240	-72.472302	OGLE SMC-LPV-881 2MASS J00301737-7228202	Mira		MIRA_SR	
7.669748	-73.712530	OGLE SMC-LPV-929 2MASS J00304075-7342450	Mira			
7.917060	-73.798217					
7.987056	-73.520435					
8.051002	-74.801395	OGLE SMC-LPV-1168 2MASS J00321227-7448049	Mira			
8.117008	-71.789106	2MASS J00322809-7147207	Can. AGB			
8.442051	-72.749582	2MASS J00334612-7244584	Can. AGB			
8.511784	-72.363404	2MASS J00340283-7221482	Can. AGB		MIRA_SR	
8.816105	-73.424329	OGLE SMC-LPV-1690 2MASS J00351587-7325275	Mira			
8.931123	-73.352948	LIN 19 2MASS J00354347-7321106	Em			
8.955451	-74.127210	2MASS J00354932-7407381	Star			
9.108186	-73.432101					
9.164485	-72.274068	2MASS J00363946-7216266	Can. AGB			
9.193053	-73.526474	MSX SMC 029 2MASS J00364631-7331351	PAGB	C		C (1) CPAGB (2) CPAGB (3)
9.230702	-74.741285					
9.236272	-72.421530	MSX SMC 091 2MASS J00365671-7225175	C			C (1) CAGB (2) CAGB (3)
9.246025	-71.636344	[FBR2002] J003659-713813	Radio			
9.328809	-72.284239	2MASS J00371893-7217031	Can. AGB			
9.384601	-73.506030	OGLE J003732.32-733021.3 2MASS J00373232-7330216	LPV			
9.387759	-72.879192	2MASS J00373306-7252451	Can. AGB			
9.446274	-73.650656	RAW 21 2MASS J00374710-7339022	C	C		
9.466017	-69.829967					
9.491884	-75.208617	[KID97] C0036-7529 2MASS J00375807-7512309	C			
9.507699	-73.790561	OGLE J003801.87-734725.7 2MASS J00380186-7347259	Mira			
9.614211	-74.260202	OGLE SMC-LPV-2488 2MASS J00382740-7415366	Mira			
9.660904	-72.008445	2MASS J00383862-7200304	Can. AGB		MIRA_SR	
9.794922	-71.569425					
9.828878	-70.131865	[MH95] 414 2MASS J00391894-7007546	C	C	MIRA_SR	
9.887294	-70.295891					
10.067795	-73.020987	OGLE J004016.25-730115.1 2MASS J00401627-7301156	Mira			
10.137255	-73.477785	OGLE J004032.93-732839.7 2MASS J00403293-7328399	Mira			
10.147153	-73.324740	OGLE J004035.31-731928.7 2MASS J00403531-7319291	Mira			

Notes. Column 1 lists the coordinates (right ascension and declination) of the source in decimal degrees. Column 2 gives some names, as listed by the SIMBAD database. A ‘?’ indicates the name of a source that is located close to the nominal position. Column 3 gives the object type, as listed by the SIMBAD database (As of January 2019. As the SIMBAD database is continuously updated this may change in time). Column 4 gives the spectral type(s), as listed in Skiff (2014). In case of many entries only a selection is listed. Column 5 gives the variable star classification as listed in the GDR2 Gaia Collaboration et al. (2018); Holl et al. (2018). Column 6 gives the classification based on the MIR *Spitzer* IRS spectra. References: (1) Groenewegen & Sloan (2018); (2) Kraemer et al. (2017); (3) Ruffe et al. (2015); (4) Jones et al. (2017); (5) Seale et al. (2009); (6) Sloan et al. (2016) (all stars listed as ‘C’ in Groenewegen & Sloan (2018), also listed in Sloan et al. 2016); (7) Woods et al. (2011). The classifications are taken directly from those papers. For the exact meaning of the abbreviations see the original papers.

Table A.2. Literature data.

RA (deg)	Dec (deg)	Type	Evo	SpT	V _m (mag)	I _m (mag)	P1 (d)	A1 (mag)	P2 (d)	A2 (mag)	VC (mag)	RC (mag)	PR (d)	AR (mag)	PB (d)	AB (mag)	erBm (mag)	erBR (mag)	erP (d)	erRm (mag)	erBR (mag)	erP1 (d)	erAR (mag)	Pother (d)	Ref.
4.876441	-72.465755																							335 ± 29	80
5.993721	-73.631895	Mira	-	-	-	17.24	479	1.6	175	0.1															
6.088240	-72.107443																								
6.498306	-73.895774	Mira	-	-	21.06	17.27	463	1.6	306	0.4															
6.795538	-73.408413	Mira	-	-	20.04	16.17	457	1.3	245	0.2															
7.329711	-71.063852																								
7.572240	-72.472302	Mira	-	-	18.23	15.84	508	1.6	202	0.1														531 ± 85	80
7.669748	-73.712530	Mira	-	-	20.77	17.80	456	1.9	211	0.3															
7.917060	-73.798217																								
7.987056	-73.520435																								
8.051002	-74.801395	Mira	-	-	20.46	17.79	495	2.0	259	0.4															
8.117008	-71.789106																								
8.442051	-72.749582																								
8.511784	-72.363404																							336 ± 37	80
8.816105	-73.424329	Mira	-	-	21.97	17.82	478	1.6	263	0.2															
8.931123	-73.352948																								
8.955451	-74.127210																								
9.108186	-73.432101																								
9.164485	-72.274068																								
9.193053	-73.526474																								
9.230702	-74.741285																							405	99
9.236272	-72.421530																								
9.246025	-71.636344																								
9.328809	-72.284239																								
9.384601	-73.506030	SRV	-	-	21.32	18.72	573	0.5	1007	0.4															
9.387759	-72.879192																								
9.446274	-73.650656																								
9.466017	-69.829967																								
9.491884	-75.208617																								
9.507699	-73.790561	Mira	-	-	18.87	15.63	511	1.4	466	0.2															
9.614211	-74.260202	Mira	-	-	20.47	16.28	463	1.5	2137	0.3															
9.660904	-72.008445																							513 ± 90	80
9.794922	-71.569425																								
9.828878	-70.131865																							343 ± 27	80
9.887294	-70.295891																								
10.067795	-73.020987	Mira	-	-	-	17.72	489	1.6	305	0.1															
10.137255	-73.477785	Mira	-	-	-	18.27	566	2.2	897	0.2															
10.147153	-73.324740	Mira	-	-	-	18.28	515	1.6	612	0.2															

Notes. Column 1 lists the right ascension and declination of the source in decimal degrees. Columns 2–10 are taken from the OGLE-III database of LPVs in the LMC and SMC (Soszyński et al. 2009a, 2011). They list the pulsation type (Mira, SRV, or OSARG) in Col. 2, and for the LMC only, the evolutionary status (AGB or RGB) and spectral type (C or O) in Cols. 3 and 4. Columns 5 and 6 list the mean magnitudes in the *V* and *I* bands. Columns 7–10 list the period and amplitude of the primary and secondary period (rounded values are listed, and the OGLE catalogue also lists a tertiary period). Columns 11–16 are taken from the analysis of MACHO data for LPVs in the LMC by (Fraser et al. 2008). Mean magnitudes in the *V* and *R* bands (in the Cousins system) are listed in Cols. 11 and 12. Period and amplitude in the red and blue band are listed in Cols. 13–16. Columns 17–23 are taken from the analysis of EROS-2 data by Kim et al. (2014) (Cols. 17–19), and Spano et al. (2011) (Cols. 20–23). Listed are the EROS *B* magnitude, the *B* – *R* colour index, and the period and its error (The error is derived from the period and the SNR of the period listed by Kim et al. 2014), respectively, the EROS *R* magnitude, the *B* – *R* colour index, the first fitted period (out of up to five periods listed in Spano et al. 2011), and the amplitude in the *R*-band. Column 24 lists other periods from the literature, with references listed in Col. 25 as follows: (34) Wood et al. (1992); (35) Whitelock et al. (2003); (36) Whitelock et al. (1989); (38) Wood et al. (1983); (43) Nishida et al. (2000); (45) Kamath et al. (2010); (80) Holl et al. (2018); (89) present work: re-analysis of the data in ref. (90); (90) Soszyński et al. (2012); (91) Ulaczyk et al. (2013); (92) Hughes (1989); (93) Payne-Gaposchkin (1971); (94) present work: re-analysis of ASAS (Pojmanski 2002) data; (95) Soszyński et al. (2009b); (96) Soszyński et al. (2008a); (97) Soszyński et al. (2008b); (98) Soszyński et al. (2010); (99) Groenewegen & Sloan (2018).

Table A.3. Results from the period analysis.

RA (deg)	Dec (deg)	χ_r^2	K (mag)	Period (d)	Amplitude (mag)	Data	References	P_{ini} (d)	Remarks
4.876441	-72.465755	19.8	11.982 \pm 0.011	265 \pm 1	0.24 \pm 0.05	32 36	1 10 11 13		Palt=333
5.993721	-73.631895	308.8	11.473 \pm 0.077	479 \pm 6	0.42 \pm 0.08	14 18	1 10 11 13	479	
6.088240	-72.107443	6.7	16.452 \pm 0.054			10 10	1		
6.498306	-73.895774	268.6	11.427 \pm 0.081	468 \pm 5	0.55 \pm 0.18	14 18	1 10 11 12 13	463	Palt=953
6.795538	-73.408413	42.2	11.455 \pm 0.025	451 \pm 5	0.32 \pm 0.12	15 18	1 11 13	457	
7.329711	-71.063852	863.7	13.422 \pm 0.227	343 \pm 4	0.73 \pm 0.38	18 24	1 10 11 13		
7.572240	-72.472302	695.6	10.792 \pm 0.062	508 \pm 12	0.39 \pm 0.18	31 33	1 10 11	508	
7.669748	-73.712530	1317.8	11.524 \pm 0.154	458 \pm 15	0.62 \pm 0.52	14 18	1 10 11 12 13	456	
7.917060	-73.798217	4.8	14.382 \pm 0.008	740 \pm 14	0.09 \pm 0.05	14 18	1 10 11 12		495
7.987056	-73.520435	1.3	14.786 \pm 0.003			15 19	1 10 11 12		
8.051002	-74.801395	48.8	11.475 \pm 0.038	491 \pm 5	0.29 \pm 0.15	13 18	1 10 11 13		
8.117008	-71.789106	70.3	11.278 \pm 0.023	600 \pm 4	0.63 \pm 0.07	17 21	1 10 11 13		
8.442051	-72.749582	175.6	12.980 \pm 0.037	571 \pm 10	0.54 \pm 0.30	15 20	1 10 11 12 13		
8.511784	-72.363404	30.2	11.622 \pm 0.025	356 \pm 1	0.70 \pm 0.04	17 23	1 10 11 13		
8.816105	-73.424329	119.3	11.139 \pm 0.039	482 \pm 5	0.46 \pm 0.07	16 22	1 10 11 12 13	478	
8.931123	-73.352948	37.8	13.720 \pm 0.016			16 23	1 10 11 12 13		
8.955451	-74.127210	1.6	14.680 \pm 0.003			18 22	1 10 11		
9.108186	-73.432101	7.5	14.453 \pm 0.008			16 19	1 10 11 12		
9.164485	-72.274068	19.7	12.326 \pm 0.011	466 \pm 2	0.43 \pm 0.05	19 22	1 10 11 13		405
9.193053	-73.526474	24.7	13.372 \pm 0.013			16 20	1 10 11 12 13		
9.230702	-74.741285	10.9	14.856 \pm 0.016	392 \pm 11	0.05 \pm 0.04	33 36	1 10 11		
9.236272	-72.421530	78.7	11.501 \pm 0.025	406 \pm 2	0.52 \pm 0.05	19 23	1 10 11 13		
9.246025	-71.636344	1.7	14.671 \pm 0.004	960 \pm 39	0.05 \pm 0.03	19 21	1 10 11		
9.328809	-72.284239	5.1	11.619 \pm 0.010	362 \pm 1	0.41 \pm 0.01	19 23	1 10 11 13		573
9.384601	-73.506030	180.6	13.187 \pm 0.046	571 \pm 16	0.42 \pm 0.33	16 20	1 10 11 12 13		
9.387759	-72.879192	28.0	13.536 \pm 0.016	686 \pm 5	0.67 \pm 0.06	16 19	1 10 11 12		
9.446274	-73.650656	605.8	13.146 \pm 0.071	992 \pm 12	1.19 \pm 0.19	34 39	1 10 11 12 13		
9.466017	-69.829967	20.3	12.504 \pm 0.027	371 \pm 2	0.55 \pm 0.05	17 22	1 10 11 13		
9.491884	-75.208617	432.8	11.599 \pm 0.098	305 \pm 3	0.41 \pm 0.20	15 19	1 10 11 13		511
9.507699	-73.790561	226.4	10.818 \pm 0.048	505 \pm 11	0.31 \pm 0.19	18 22	1 10 11 13		
9.614211	-74.260202	70.8	11.272 \pm 0.033	448 \pm 2	0.49 \pm 0.12	18 21	1 10 13	463	
9.660904	-72.008445	111.4	11.029 \pm 0.036	385 \pm 8	0.25 \pm 0.31	19 23	1 10 11 13		
9.794922	-71.569425	42.1	14.554 \pm 0.017			19 23	1 10 11 13		
9.828878	-70.131865	356.8	11.624 \pm 0.384	320 \pm 4	0.51 \pm 0.38	17 20	1 10 11 13		long term drop
9.887294	-70.295891	428.8	11.502 \pm 0.132	386 \pm 6	0.35 \pm 0.21	17 21	1 10 11 13		
10.067795	-73.020987	291.6	11.568 \pm 0.056	482 \pm 7	0.43 \pm 0.23	16 19	1 10 11	489	
10.137255	-73.477785	100.0	11.423 \pm 0.032	566 \pm 5	0.34 \pm 0.04	16 22	1 10 11 12 13	566	
10.147153	-73.324740	75.1	12.085 \pm 0.028	507 \pm 3	0.55 \pm 0.07	16 21	1 10 11 13	515	

Notes. Column 1 lists the coordinates (right ascension and declination) of the source in decimal degrees. Column 2 Lists the reduced χ^2 statistics. Column 3 lists the mean K -band magnitude. Column 4 lists the pulsation period with error. Column 5 lists the amplitude in the K -band. Column 6 lists the number of available data points. The first number indicates the number from the VMC survey, the second the total number. Column 7 lists the references for the available data points as follows, (1) present work from the VMC survey; (10) 2MASS (Cutri et al. 2003) (11) 2MASS 6X (Cutri et al. 2012) (12) IRSF (Kato et al. 2007) (13) DENIS Consortium (2005) (31) Zijlstra et al. (1996); (32) van Loon et al. (1997); (33) Reid (1991); (34) Wood et al. (1992); (35) Whitelock et al. (2003); (36) Whitelock et al. (1989); (37) Peter Wood and Greg Sloan (private communication 2016); (38) Wood et al. (1983); (39) Hughes & Wood (1990); (40) Reid et al. (1995); (41) Reid et al. (1990); (42) Glass & Reid (1985); (43) Nishida et al. (2000); (44) Frogel et al. (1990); (45) Kamath et al. (2010); (46) Groenewegen & Blommaert (1998); (47) Tanabé et al. (1997); (48) Ferraro et al. (1995). Column 8 gives the initial period used in the LC fitting (overwriting any period found from the Fourier analysis). This value comes from the literature, see Table A.2. Column 9 lists any remarks on the source or the LC fitting. Sometimes possible alternative periods are given ('Palt'), or the long secondary period ('Plsp').

Table C.1. SED and spectra fitted to some non-AGB stars.

RA (deg)	Dec (deg)	Name	SIMBAD Object type	IRS Classification	Reference	Adopted classification
72.90	−67.08	SMP LMC 11	PN	CPAGB (4)	Sanduleak et al. (1978)	PN
81.51	−67.49	HD 36402	WR	WR (4)	Westerlund & Smith (1964)	WR
81.05	−68.49	IRAS 05244 – 6832	YSO	HII (4), HII (7)	Kastner et al. (2008)	H II
13.53	−72.69	LHA 115-S 18	Em	Be (2), B[e] star (3)	Zickgraf et al. (1989)	Be
74.40	−67.79	LHA 120-S 12	BSG	B[e] (4)	Zickgraf et al. (1986)	Be
74.19	−69.84	HD 268835	BSG	B[e] (4)	Zickgraf et al. (1986)	Be
78.70	−67.20	IRAS 05148 – 6715	YSO	YSO1 (4), YSO1 (7)	Oliveira et al. (2009)	YSO
83.16	−69.51	[RP2006] 774	YSO	YSO4 (4), YSO4 (7)	Gruendl & Chu (2009); Reid (2014)	YSO
84.00	−67.75	2MASS J05360241 – 6745171	YSO candidate	YSO4 (4), YSO4 (7)	Reid (2014)	YSO
85.14	−69.41	2MASS J05403400 – 6925099	YSO	YSO4 (4), O Group (5)	Seale et al. (2009)	YSO
73.19	−69.19	IRAS 04530 – 6916	YSO candidate	B[e] (4), F Group (5)	Seale et al. (2009)	YSO
80.37	−67.85	IRAS 05216 – 6753	PN	H II (4)	Whitney et al. (2008)	YSO (?)

Notes. Column 1 gives the right ascension and declination. Column 2 gives the name of the object. Column 3 gives the object type listed in SIMBAD. Column 4 gives the classification based on the IRS spectrum, copied from Table A.1. References are: (2) Kraemer et al. (2017); (3) Ruffle et al. (2015); (4) Jones et al. (2017); (5) Seale et al. (2009); (7) Woods et al. (2011). Column 5 gives a reference supporting the adopted classification listed in Col. 6.

Appendix C.2: Fitting the SEDs to the templates

Given a template with luminosity (L_t), distance (d_t) and synthetic absolute magnitudes in many filters (M_t) and an object with observed absolute magnitudes with errors (M_o, σ) for an assumed distance (d_o), the comparison between template and object is

$$\chi^2 = \sum ((M_t + o - M_o)/\sigma)^2, \quad (\text{C.1})$$

where the sum runs over the observed magnitudes in different filters. As the template was originally fitted to the photometric and spectroscopic data of a star for a certain distance resulting in a best-fitting luminosity there is a degeneracy as a template could fit any observed SED by a simple offset (o) in magnitude.

Setting the derivative of χ^2 to zero, the offset that will provide the best fit is

$$o = \sum (m_t - m_o)/\sigma^2, \quad (\text{C.2})$$

that is the weighted mean difference between observed and template magnitudes.

The SEDs of the 254 targets are compared in this way to a total of 374 templates. As additional constraint it was imposed that in order to be a valid template a C-star had to have a predicted luminosity above 1 000 L_\odot and below 70 000 L_\odot , an O-rich AGB star to be above 500 L_\odot and for an O-rich RSG to be above 5 000 L_\odot . This results in an ordered list of χ^2 s with the type of the template, and the luminosity of the target (for an assumed distance of 50 kpc to the LMC and 61 kpc for the objects in the SMC).

There are 50 objects among the 254 that were fitted by GS18. This allows to check the level of ‘contamination’: if a star is a known C-rich object, is the best-fitting template that of a C-star, and at what level of χ^2 is a non-C star considered a possible match. This is not a trivial exercise as the SEDs used in GS18 and constructed here are not the same. For example, GDR2 photometry and VMC magnitudes were not used by GS18. Instead NIR photometry was taken from the available 2MASS, 2MASS6X, IRSF, and DENIS data. In addition the fits in GS18 were made to the photometry and *Spitzer* spectra, which leads to different synthetic magnitudes than if only the photometry were fitted as is done here. Among the 35 known C-stars the best fitting template is always that of a C-star and the best-fitting O-rich template has a χ^2 that is (when ordered) 1.36, 1.99, 2.05, ... times larger than the χ^2 of the best matching template. Among the 15

known O-rich stars the best fitting template is always that of an O-rich star and the best-fitting C-rich template has a χ^2 that is 1.28, 1.31, 1.32, 1.51, 1.65, ... times larger than the χ^2 of the best matching template.

Based on this result, the list of templates with a χ^2 less than 1.5 times that of the best-fitting template is retained and used in the classification. In this case, 34 stars are classified as ‘C’ (all templates are of C-stars), one as ‘C (AGB)’ (the best fitting template is C, and the alternative(s) is (are) (an) O-rich AGB stars or RSGs), 12 as ‘O’ (all templates are O-rich AGB stars or RSGs), and 3 as ‘O (AGB)’ (the best fitting template is that of an O-rich AGB star or RSG, and the alternative(s) is (are) C-stars).

The finding that the classification of AGB stars based on a fit to the SED gives reliable results, and that the success rate of classification is better for C-stars than for O-stars was also found by Gullieuszik et al. (2012). They fitted the SEDs of 374 stars in one VMC field selected to be AGB stars based on CCDs and CMDs both with a C-star atmosphere model and carbonaceous dust grains, and an O-star model and silicate dust grains and selected the best model based on a χ^2 comparison. Eighty-seven stars in the field were spectroscopically identified as C-stars and the SED fitting classified 87% of them correctly, even 100% for stars with $(J - K_s) > 1.5$ mag. They also fitted the SEDs of stars with a known classification from *Spitzer* spectra in the MCs. The classification was correct in more than 90% of the cases for C-stars and about 75% for the O-rich stars.

If among the list of templates there is a non-AGB star this is marked by OTHER, for example, ‘C(OTH)’. The best-fitting template could be a YSO, and in that case one could have the classification ‘YSO’ (all templates are those of YSOs), ‘YSO(AGB)’ (the best fitting template is that of a YSO, and the alternatives are only O-rich AGB stars, RSGs, or C-rich stars), or ‘YSO(OTH)’ (the best fitting template is that of a YSO, and the alternatives could be (an) AGB star(s), RSG(s), WR, Be star, HII, or PN).

The results of the template fitting are listed in Col. 10 in Table C.2 with the predicted luminosity in Col. 11 (the error in L is estimated to be 15% based on the typical scatter in luminosity among the best-fitting templates). The SEDs of all 254 objects with their best matching templates are plotted in Fig. C.2. In total 197 stars are classified as C-rich (in 2 cases the matching templates include O-rich stars, and in 3 cases the matching templates include ‘other’ objects). The luminosities are between

1000 and 29 000 L_{\odot} , in agreement with GS18 who derived luminosities for 225 C-stars between 1125 and 56 700 L_{\odot} . All three objects marked as ‘C(OTH)’ are at relatively low luminosities between 1250 and 2850 L_{\odot} and based on a visual inspection of their SED and additional information (one object is classified as an emission-line object) the three are classified as likely non-AGB stars. In total 22 stars are classified as O-rich (in 5 cases the matching templates include C-rich stars, and in 2 cases the matching templates include ‘other’ objects). The luminosities are between 7000 and 98 000 L_{\odot} with one exception (1500 L_{\odot}) in agreement with GS18. For 82 stars classified as O-rich AGB stars they found a range between 1500 and 107 000 L_{\odot} and for 76 stars they classified as RSG a range from 24 500 to \sim 250 000 L_{\odot} . That means that 217 stars are very likely AGB stars and the period analysis has revealed LPV like properties.

Twenty stars are classified as YSOs, in 5 cases AGB stars are among the best-fitting templates. Fifteen have luminosities between 400 and 2800 L_{\odot} while five have luminosities between 4500 and 20 000 L_{\odot} . Two stars are classified as PNe, six as HII regions and seven as Be-stars.

Appendix D: Results of the fits to synthetic spectra from Nanni et al. (2019)

Table D.1 lists the first entries of the table available at the CDS. It provides the results of the SED fitting performed to synthetic spectra from Nanni et al. (2019) for the 217 objects classified as AGB stars in this work.

The calculation of the uncertainty on the MLR and luminosity is the same as that described by Nanni et al. (2018, 2019). The synthetic photometry that best fits the observations provides $\chi^2 = \chi^2_{\text{best}}$. Each of the synthetic fluxes are randomly modified within the observed flux errors, and a new value of χ^2 between the observed and modified flux is calculated. Such a procedure is reiterated 100 times and an equal number of χ^2 values are computed. From the 100 χ^2 we extract the minimum and the 34th values (corresponding to 1σ). The difference between the minimum and the 1σ value provides the statistical variation of $\Delta\chi^2$ and thus the maximum acceptable value of χ^2 , $\chi^2_{\text{max}} = \chi^2_{\text{best}} + \Delta\chi^2$. We then select from the grid of models those that yield a value of χ^2 : $\chi^2 \leq \chi^2_{\text{max}}$, and we compute their average and standard deviation, which provides the corresponding uncertainty of the quantity calculated. If fewer than 4 models satisfy the condition $\chi^2 \leq \chi^2_{\text{max}}$, the stellar quantities are assumed to be represented by the best-fitting value and zero uncertainty.

Table D.1. Results from the SED fitting performed to synthetic spectra from Nanni et al. (2019) for all AGB candidates selected in this work.

RA (deg)	Dec (deg)	Name	\dot{M} ($10^{-6} M_{\odot} \text{ yr}^{-1}$)	Luminosity (L_{\odot})
4.876441	-72.465755	2MASS J00193036-7227567	1.76 ± 0.67	3162
8.117008	-71.789106	2MASS J00322809-7147207	5.0 ± 1.5	7943
8.442051	-72.749582	2MASS J00334612-7244584	7.94	7943
8.511784	-72.363404	2MASS J00340283-7221482	2.51	3981
9.164485	-72.274068	2MASS J00363946-7216266	3.16	5012
9.236272	-72.421530	MSX SMC 091 2MASS J00365671-7225175	3.08 ± 0.54	5012
9.328809	-72.284239	2MASS J00371893-7217031	1.72 ± 0.54	3162
9.387759	-72.879192	2MASS J00373306-7252451	11.22	5012
9.466017	-69.829967		2.57 ± 0.58	3162
9.828878	-70.131865	[MH95] 414 2MASS J00391894-7007546	1.85 ± 0.33	3981
9.887294	-70.295891		1.58	5012
10.466052	-71.648376	2MASS J00415184-7138541	2.98 ± 0.63	3981
10.590777	-72.401692	2MASS J00422179-7224060	1.59 ± 0.49	3981
10.803761	-72.249720	2MASS J00431291-7214590	2.0	3981
11.433544	-72.137625	2MASS J00454404-7208154	1.92 ± 0.36	3981
11.844981	-74.952560	2MASS J00472280-7457092	1.00	2512
12.148646	-74.177498	IRAS F00468-7427 2MASS J00483568-7410391	15.8 ± 4.2	6310
12.529927	-73.523596	IRAS 00483-7347 2MASS J00500719-7331251	37.3 ± 2.6	25120
12.627578	-72.858313	IRAS F00486-7308 2MASS J00503062-7251298	4.35 ± 1.55	25120
12.707210	-73.815508	2MASS J00504974-7348557	14.13 ± 3.23	5012
13.332679	-75.138802	OGLE J005337.29-723434.9	2.12 ± 0.56	5012
13.595669	-74.832455		13.19 ± 3.48	5012
13.791431	-73.712404	2MASS J00550995-7342447	9.1 ± 3.2	3981
13.923324	-70.409980	2MASS J00554160-7024359	3.2 ± 1.1	5012
14.860307	-72.394923	2MASS J00592646-7223417	5.01	3981
15.058298	-74.958569		1.58	3981
15.173262	-72.633511	2MASS J01004152-7238003	2.9 ± 1.0	2081 ± 211
15.194747	-74.420436	2MASS J01004675-7425136	1.85 ± 0.33	3162
15.636536	-72.320172	2MASS J01023277-7219125	3.56 ± 1.16	3981
15.851503	-72.634413	SAGEM A J010324.38-723803.8	1.36 ± 0.28	20560 ± 1220
15.891398	-72.734837	2MASS J01033393-7244053	1.00	14130
15.893094	-70.597998	2MASS J01033435-7035528	3.04 ± 0.70	6310
15.941578	-75.266262		5.34 ± 0.65	12590
16.062660	-70.405257	SAGEM A J010415.07-702418.9	10.7 ± 1.7	5012
17.634352	-73.084464	IRAS F01091-7320 2MASS J01103224-7305040	7.94	6310
19.320585	-74.804827	2MASS J01171696-7448173	2.0	3162
19.322041	-74.604738	IRAS F01160-7451 2MASS J01171728-7436170	11.2	11220
20.617749	-71.157234	IRAS F01210-7125 2MASS J01222827-7109260	6.7 ± 2.7	11220
21.130633	-71.620707	2MASS J01243139-7137145	2.51	3981
22.765869	-71.318003	2MASS J01310381-7119048	5.11 ± 0.36	7943
23.417313	-73.823852	2MASS J01334016-7349257	10.0	7943
24.195532	-72.641560	2MASS J01364695-7238295	3.16	6310
25.517064	-75.171631	2MASS J01420412-7510177	1.26	3162
66.778920	-73.458705		4.23 ± 0.98	6310
68.402239	-67.659170	2MASS J04333653-6739329	7.94	5012
68.629927	-70.830315		3.52 ± 0.67	6310
68.850394	-66.947047	2MASS J04352409-6656493	3.00 ± 0.33	3981
69.049993	-71.370090	2MASS J04361200-7122123	10.0 ± 1.2	13668 ± 744
69.178078	-68.536224	MSX LMC 1045	2.51	5012
69.781620	-74.922266		3.16	6310
70.088825	-75.332959		15.2 ± 2.5	5012
70.104244	-74.743169		3.26 ± 0.89	5012
70.118694	-69.920432	IRAS 04407-7000 2MASS J04402848-6955135	14.4 ± 3.0	22390
70.438656	-72.645357	2MASS J04414529-7238431	5.1 ± 1.1	3981
70.632433	-74.796568		1.26	3162
71.369404	-72.260494	2MASS J04452864-7215379	10.7 ± 2.8	5012

Notes. Column 1 lists the right ascension and declination of the source in decimal degrees. Column 2 gives some names, copied from Table A.1. Column 3 lists the MLR. Column 4 lists the luminosity.

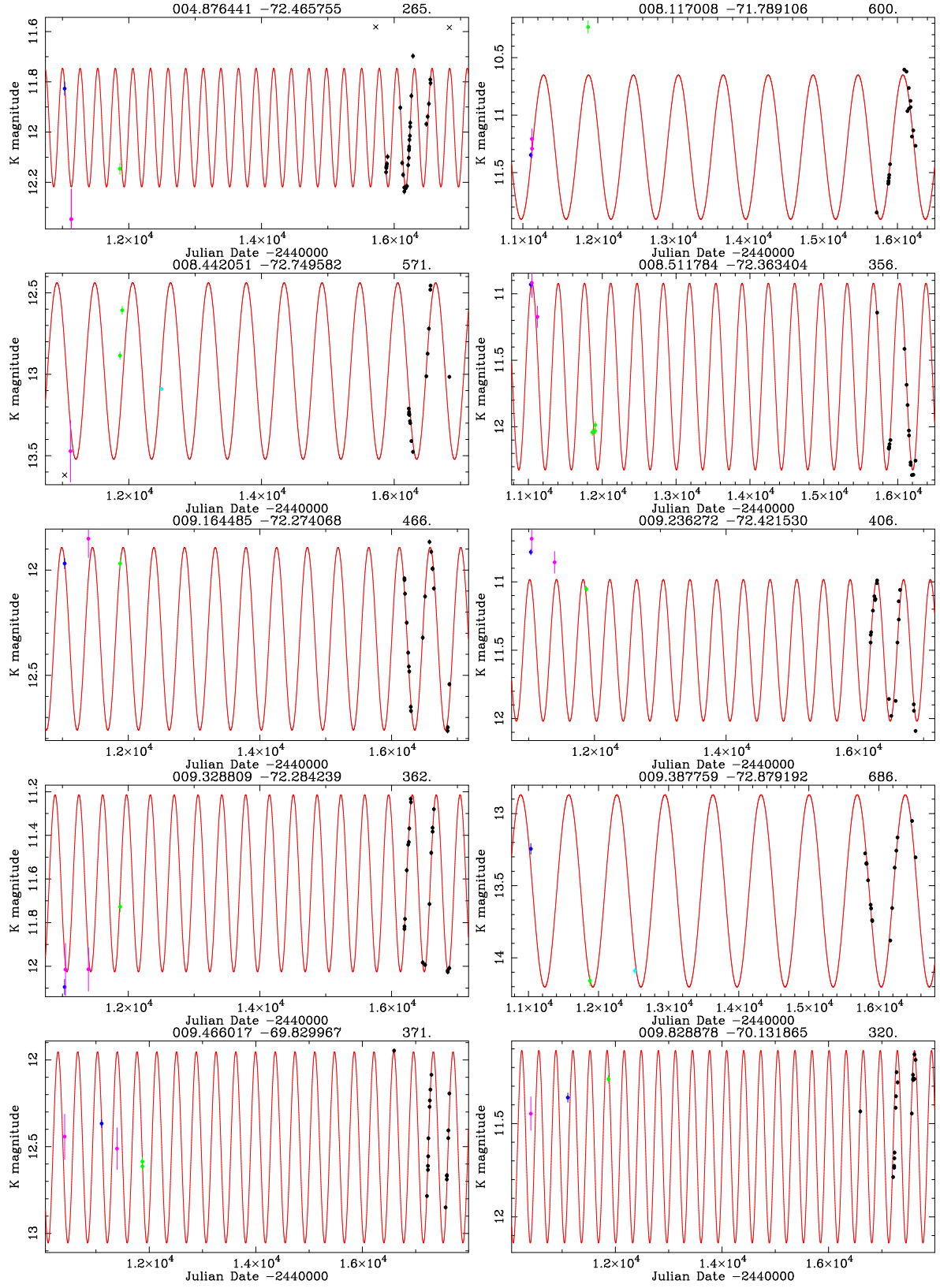


Fig. A.1. Examples of the LC fitting (red solid lines) to the observed time photometry. On top of the plot the identifier and the period (in days) are listed. Data points (with error bars) are identified as follows: black: VMC, green: 2MASS, dark blue: 2MASS-6X, light blue: IRSF, magenta: DENIS, orange: other sources (see references in the footnote to Table A.3). Black crosses indicate points excluded from the fits.

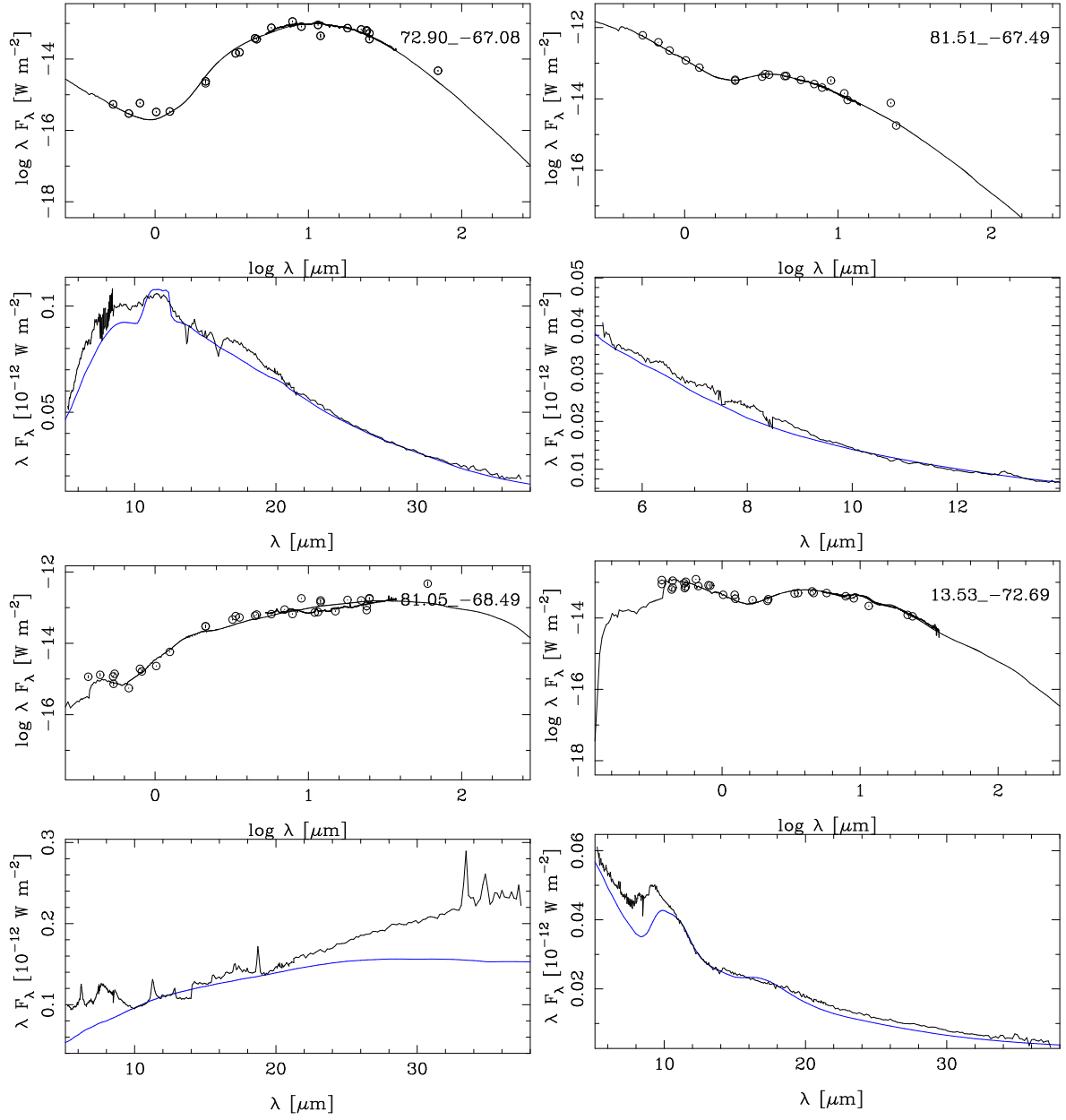


Fig. C.1. SEDs and *Spitzer* spectra of a C-rich post-AGB/PN star (top left), a Wolf-Rayet star (top right), an HII region (bottom left) and a Be star (bottom right). See the notes to Table C.1 for the spectroscopic classification. In the panels with the *Spitzer* IRS spectra, the models (blue lines) are scaled to the observed spectra based on the average flux in the 12–13 μm region. For simplicity, the identifiers are the RA and Dec from Table A.1 truncated to two decimal figures.

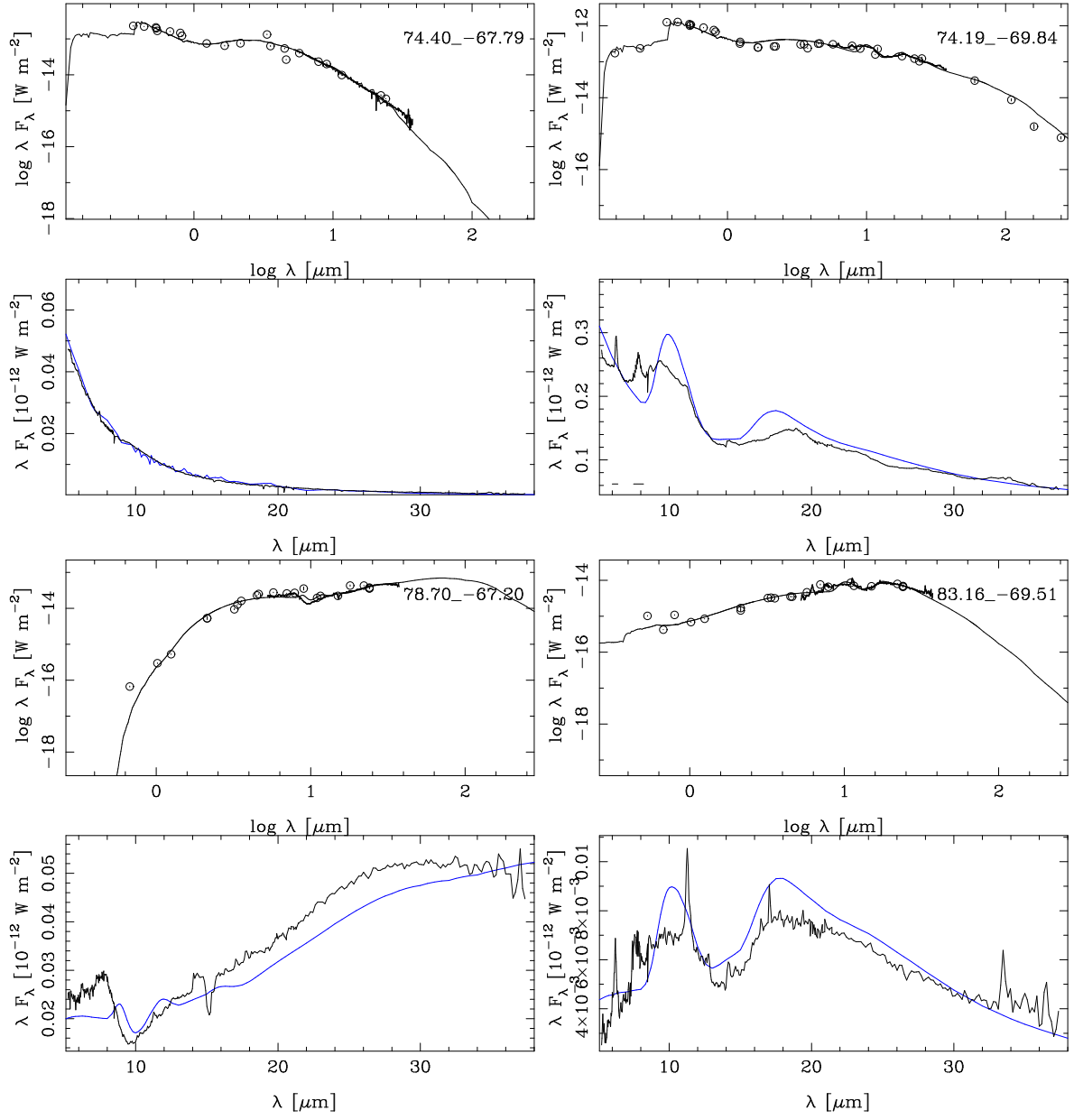


Fig. C.1. Continued. The SEDs and *Spitzer* spectra of two Be stars (top panels) and two YSOs (bottom panels). See the notes to Table C.1 for the spectroscopic classification.

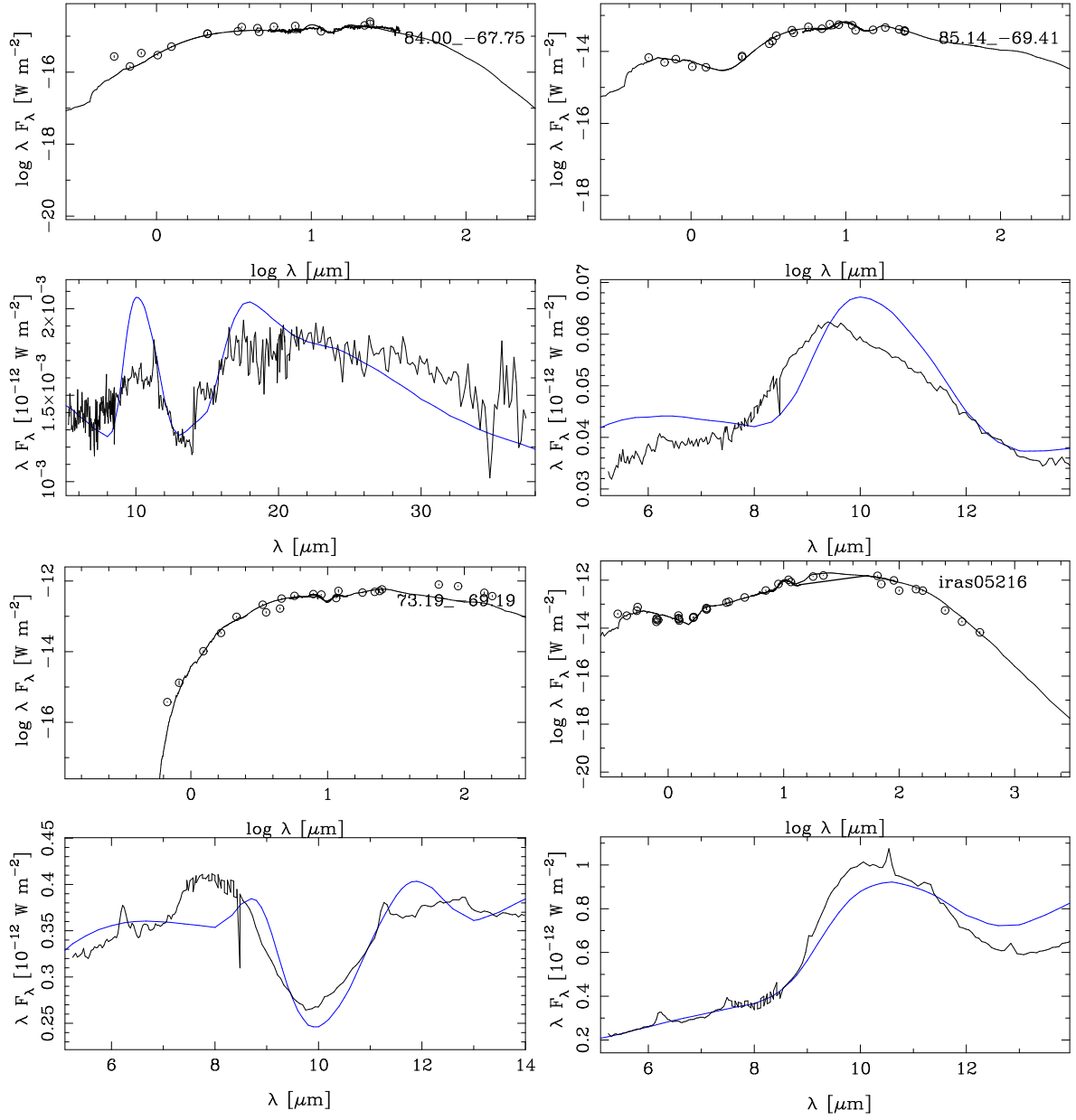


Fig. C.1. Continued. The SEDs and *Spitzer* spectra of four YSOs. See the notes to Table C.1 for the spectroscopic classification.

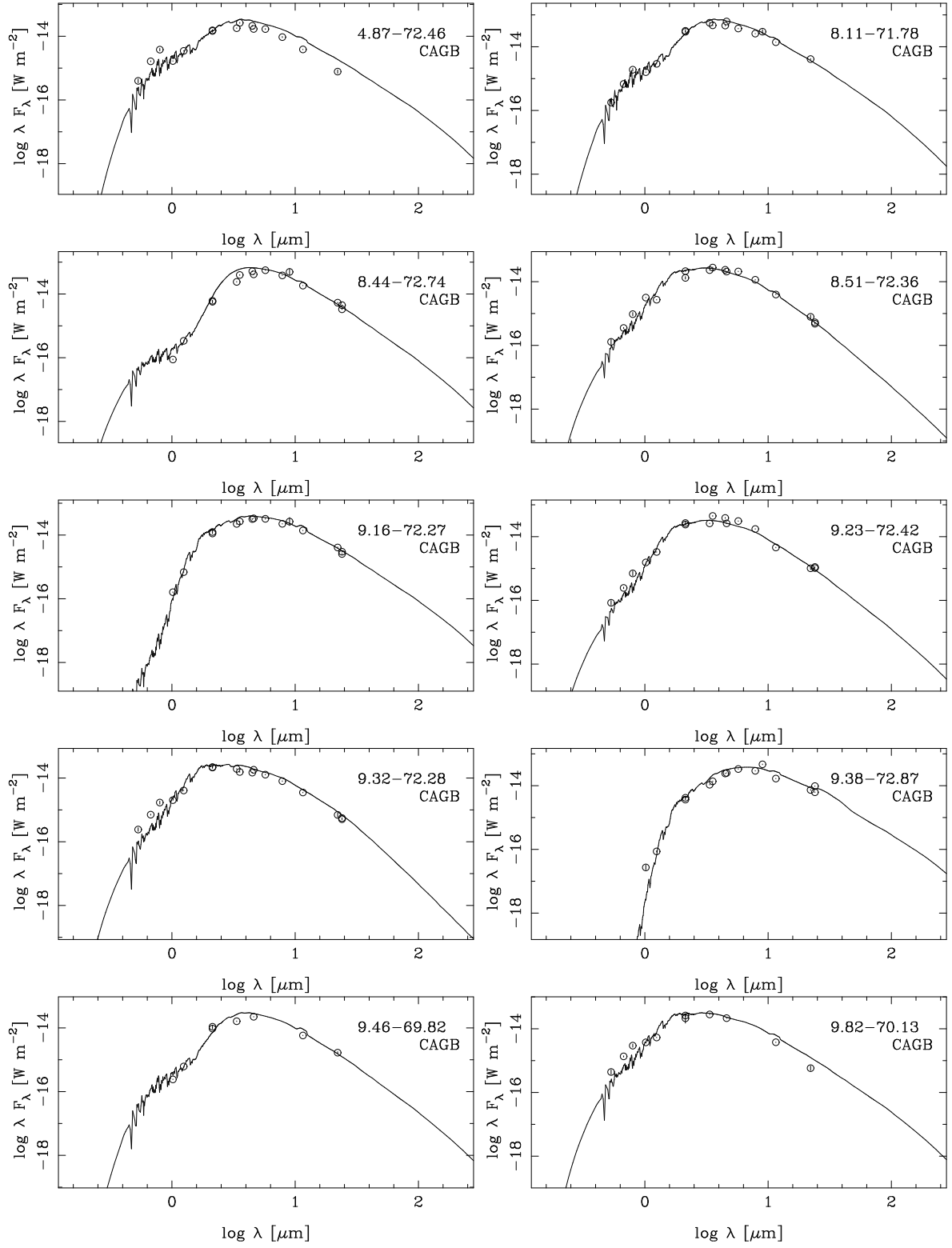


Fig. C.2. Examples of the fitting of a template (the solid line) to the observed photometry. The top right corner lists the identifier of the star (RA and Dec truncated to two decimal figures), and below it the type of the template.

Table C.2. Sample of stars with fitted energy distributions.

RA (deg)	Dec (deg)	Name	Obj. Type	Sp. Type	IRS	K (mag)	Period (d)	Amp (mag)	χ_r^2	SED T	SED L (L_\odot)
Most likely AGB stars and LPVs											
4.876441	-72.465755	2MASS J00193036-7227567	Can. AGB			11.982 \pm 0.011	265 \pm 1 ^a	0.24 \pm 0.05	19.8	C	4530
8.117008	-71.789106	2MASS J00322809-7147207	Can. AGB			11.278 \pm 0.023	600 \pm 4	0.63 \pm 0.07	70.3	C	9231
8.442051	-72.749582	2MASS J00334612-7244584	Can. AGB			12.980 \pm 0.037	571 \pm 10	0.54 \pm 0.30	175.6	C	8462
8.511784	-72.363404	2MASS J00340283-7221482	Can. AGB			11.622 \pm 0.025	356 \pm 1	0.70 \pm 0.04	30.2	C	4719
9.164485	-72.274068	2MASS J00363946-7216266	Can. AGB			12.326 \pm 0.011	466 \pm 2	0.43 \pm 0.05	19.7	C	5802
9.236272	-72.421530	MSX SMC 091 2MASS J00365671-7225175	C		C(1)	11.501 \pm 0.025	406 \pm 2	0.52 \pm 0.05	78.7	C	5698
9.328809	-72.284239	2MASS J00371893-7217031	Can. AGB			11.619 \pm 0.010	362 \pm 1	0.41 \pm 0.01	5.1	C	3959
9.387759	-72.879192	2MASS J00373306-7252451	Can. AGB			13.536 \pm 0.016	686 \pm 5	0.67 \pm 0.06	28.0	C	5789
9.466017	-69.829967					12.504 \pm 0.027	371 \pm 2	0.55 \pm 0.05	20.3	C	3655
9.828878	-70.131865	[MH95] 414 2MASS J00391894-7007546	C	C		11.624 \pm 0.384	320 \pm 4	0.51 \pm 0.38	356.8	C	4919
9.887294	-70.295891					11.502 \pm 0.132	386 \pm 6	0.35 \pm 0.21	428.8	C	6494
10.466052	-71.648376	2MASS J00415184-7138541	Can. AGB			12.075 \pm 0.060	374 \pm 6	0.70 \pm 0.18	290.2	C	4004
10.590777	-72.401692	2MASS J00422179-7224060	C			11.456 \pm 0.046	327 \pm 2	0.37 \pm 0.12	112.0	C	4707
10.803761	-72.249720	2MASS J00431291-7214590	Can. AGB			12.449 \pm 0.012	411 \pm 1	0.35 \pm 0.05	17.2	C	5351
11.433544	-72.137625	2MASS J00454404-7208154	Can. AGB			11.578 \pm 0.113	351 \pm 5	0.39 \pm 0.08	424.2	C	4460
11.844981	-74.952560	2MASS J00472280-7457092	Can. AGB			12.266 \pm 0.038	326 \pm 2	0.48 \pm 0.07	50.3	C	3107
12.148646	-74.177498	IRAS F00468-7427 2MASS J00483568-7410391	C	C		14.481 \pm 0.012	727 \pm 3	0.69 \pm 0.06	11.2	C	6432
12.529927	-73.523596	IRAS 00483-7347 2MASS J00500719-7331251	Mira	M8	MA(1)	8.736 \pm 0.016	2075 \pm 15	0.32 \pm 0.02	1.3	O	80128
12.627578	-72.858313	IRAS F00486-7308 2MASS J00503062-7251298	Mira	M8II		8.953 \pm 0.054	1062 \pm 10	0.56 \pm 0.05	3.2	O	39334
12.707210	-73.815508	2MASS J00504974-7348557	IR			14.770 \pm 0.034	1252 \pm 6 ^a	1.06 \pm 0.06	13.8	C	5548
13.332679	-75.138802	OGLE J005337.29-723434.9	Mira			11.434 \pm 0.037	499 \pm 4	0.42 \pm 0.11	102.4	C	5753
13.595669	-74.832455					14.834 \pm 0.018	717 \pm 7	0.39 \pm 0.12	19.0	C	5085
13.791431	-73.712404	2MASS J00550995-7342447	Can. AGB			13.755 \pm 0.032	309 \pm 1	0.62 \pm 0.06	101.1	C	4666
13.923324	-70.409980	2MASS J00554160-7024359	Can. AGB			11.221 \pm 0.021	804 \pm 25	0.21 \pm 0.08	107.1	C	6504
14.860307	-72.394923	2MASS J00592646-7223417	Can. AGB			13.110 \pm 0.047	434 \pm 3	0.52 \pm 0.20	196.2	C	4343
15.058298	-74.958569					11.685 \pm 0.042	427 \pm 4	0.38 \pm 0.13	67.7	C	4284
15.173262	-72.633511	2MASS J01004152-7238003	Can. AGB			15.139 \pm 0.074	451 \pm 7	0.37 \pm 0.15	141.5	C	2432
15.194747	-74.420436	2MASS J01004675-7425136	Can. AGB			11.961 \pm 0.049	903 \pm 10	0.74 \pm 0.13	213.8	C	4360
15.636536	-72.320172	2MASS J01023277-7219125	Can. AGB			13.348 \pm 0.013	576 \pm 2	0.72 \pm 0.06	28.7	C	5020
15.851503	-72.634413	SAGEMMA J010324.38-723803.8	Can. PAGB			11.130 \pm 0.062	673 \pm 21	0.43 \pm 0.34	372.7	O(AGB)	31147
15.891398	-72.734837	2MASS J01033393-7244053	Can. AGB			11.399 \pm 0.032	663 \pm 10	0.26 \pm 0.14	92.8	O	18107
15.893094	-70.597998	2MASS J01033435-7035528	Can. AGB			11.316 \pm 0.043	1088 \pm 17	0.36 \pm 0.17	195.9	C	8451
15.941578	-75.266262					11.247 \pm 0.043	617 \pm 6	0.45 \pm 0.20	124.1	C	14608
16.062660	-70.405257	SAGEMMA J010415.07-702418.9	Can. AGB			15.291 \pm 0.044	1317 \pm 52	0.75 \pm 0.33	164.5	C	5217
17.634352	-73.084464	IRAS F01091-7320 2MASS J01103224-7305040	C	C		13.109 \pm 0.028	502 \pm 2	0.58 \pm 0.02	44.8	C	6375
19.320585	-74.804827	2MASS J01171696-7448173	Can. AGB			11.588 \pm 0.108	353 \pm 2	0.62 \pm 0.12	82.2	C	4060
19.322041	-74.604738	IRAS F01160-7451 2MASS J01171728-7436170	Can. AGB			11.615 \pm 0.020	586 \pm 3	0.55 \pm 0.07	42.2	C	13101
20.617749	-71.157234	IRAS F01210-7125 2MASS J01222827-7109260	C	C		10.579 \pm 0.102	620 \pm 10	0.67 \pm 0.14	4.1	C	11536
21.130633	-71.620707	2MASS J01243139-7137145	Can. AGB			11.871 \pm 0.047	724 \pm 12	0.56 \pm 0.26	244.8	C	3623
22.765869	-71.318003	2MASS J01310381-7119048	Can. AGB			10.927 \pm 0.010	643 \pm 2	0.38 \pm 0.04	11.1	C	9858
23.417313	-73.823852	2MASS J01334016-7349257	Can. AGB			12.529 \pm 0.108	474 \pm 8	0.69 \pm 0.10	398.1	C	9148
24.195532	-72.641560	2MASS J01364695-7238295	Can. AGB			11.215 \pm 0.022	487 \pm 2	0.47 \pm 0.07	39.6	C	8192
25.517064	-75.171631	2MASS J01420412-7510177	Can. AGB			11.557 \pm 0.030	272 \pm 1	0.51 \pm 0.09	84.2	C	3805
66.778920	-73.458705					11.071 \pm 0.027	469 \pm 2	0.37 \pm 0.07	36.7	C	5926
68.402239	-67.659170	2MASS J04333653-6739329	Star			13.406 \pm 0.022	676 \pm 5	0.88 \pm 0.11	58.1	C	4624
68.629927	-70.830315					10.725 \pm 0.025	447 \pm 3	0.42 \pm 0.02	56.8	C	6998
68.850394	-66.947047	2MASS J04352409-6656493	Star		C(1)	13.117 \pm 0.055	600 \pm 9	0.76 \pm 0.12	346.5	C	3740

Groenewegen et al.: Pulsation periods of enshrouded AGB stars in the Magellanic Clouds

Table C.2. continued.

RA (deg)	Dec (deg)	Name	Obj. Type	Sp. Type	IRS	K (mag)	Period (d)	Amp (mag)	χ_r^2	SED T	SED L (L_\odot)
69.049993	-71.370090	2MASS J04361200-7122123	Star			11.481 ± 0.116	804 ± 10	0.72 ± 0.22	166.4	C	13052
69.178078	-68.536224	MSX LMC 1045	AGB			11.704 ± 0.024	461 ± 3	0.50 ± 0.08	83.6	C	5719
69.781620	-74.922266					11.260 ± 0.081	1891 ± 24^b	0.84 ± 0.26	147.4	C	5687
70.088825	-75.332959					13.076 ± 0.034	763 ± 9	0.99 ± 0.14	39.1	C	5649
70.104244	-74.743169					11.251 ± 0.100	1035 ± 19	0.37 ± 0.10	109.1	C	5395
70.118694	-69.920432	IRAS 04407-7000 2MASS J04402848-6955135	Mira	M1.5	MA(1)	8.756 ± 0.018	1185 ± 5	0.60 ± 0.04	4.2	O	30030
70.438656	-72.645357	2MASS J04414529-7238431	Star			14.136 ± 0.158	686 ± 21	0.66 ± 0.33	55.6	C	4011
70.632433	-74.796568					11.573 ± 0.062	$3108 \pm 29^{a,b}$	0.79 ± 0.12	18.0	C	3570
71.369404	-72.260494	2MASS J04452864-7215379	Star			15.539 ± 0.047	614 ± 11	0.77 ± 0.08	61.5	C	5220
71.385232	-75.123398					11.350 ± 0.088	527 ± 3	0.30 ± 0.08	36.0	C	5060
71.628126	-71.703265					11.546 ± 0.050	926 ± 15	0.26 ± 0.10	105.2	C	5341
71.817568	-72.884156	2MASS J04471623-7253029	Star			11.700 ± 0.016	530 ± 3	0.38 ± 0.06	26.3	C	8590
72.115146	-69.889676	SAGE1C J044827.59-695322.9	AGB			15.939 ± 0.031	571 ± 7	0.85 ± 0.06	39.1	C	5453
72.332262	-71.271020	IRAS 04498-7121 2MASS J04491975-7116155	AGB			12.287 ± 0.039	636 ± 12	0.69 ± 0.13	297.8	C	8609
72.374867	-74.743909					14.200 ± 0.105	408 ± 8^a	0.84 ± 0.25	56.8	C	3684
72.422730	-68.630912	IRAS 04498-6842 2MASS J04494147-6837514	Mira	M10	MA(1)	8.073 ± 0.023	1245 ± 9	0.64 ± 0.03	4.5	O	56186
72.668585	-69.292201	IRAS 04509-6922 2MASS J04504046-6917319	Mira	M10	MA(1)	8.550 ± 0.023	1259 ± 6	0.72 ± 0.04	5.5	O(AGB)	36290
72.870832	-68.963902	IRAS 04516-6902 2MASS J04512899-6857500	Mira	M9	MA(1)	8.730 ± 0.025	1092 ± 7	0.77 ± 0.06	7.6	O	46865
73.046582	-70.212454	2MASS J04521119-7012448	Can. PAGB			12.508 ± 0.015	2510 ± 67	0.15 ± 0.06	14.4	C	2986
73.084066	-68.725016	MSX LMC 1213 2MASS J04522017-6843301	AGB		C(1)	12.755 ± 0.027	481 ± 3	0.64 ± 0.09	89.8	C	4656
73.225797	-72.351528	MSX LMC 1347	Star			14.925 ± 0.049	713 ± 14	0.94 ± 0.32	112.5	C	7163
73.309090	-65.793953	2MASS J04531419-6547383	Star			13.259 ± 0.037	606 ± 5	0.82 ± 0.04	155.0	C	4578
73.506857	-72.031374					12.384 ± 0.048	328 ± 3	0.60 ± 0.10	82.1	C	3596
73.541954	-69.932864	IRAS 04545-7000 2MASS J04541005-6955582	AGB		MA(1)	10.238 ± 0.041	1239 ± 10	0.83 ± 0.06	24.0	O(AGB)	25752
73.835407	-68.377557	MSX LMC 1210 2MASS J04552049-6822391	Mira			9.385 ± 0.047	1075 ± 9	0.54 ± 0.06	3.7	O(OTH)	31031
74.056294	-69.541896	[GC2009] J045613.48-693231.1	YSO			17.078 ± 0.090	514 ± 17	0.74 ± 0.29	52.7	C	5558
74.108187	-71.424526	2MASS J04562597-7125282	Star			13.146 ± 0.031	764 ± 6	0.40 ± 0.01	25.5	C	8341
74.197446	-70.615018	2MASS J04564739-7036540	Star			12.903 ± 0.043	752 ± 5	0.71 ± 0.10	103.6	C	8164
74.322305	-70.222714	MSX LMC 1333 2MASS J04571732-7013216	AGB			12.222 ± 0.021	643 ± 5	0.69 ± 0.12	65.6	C	9117
74.439693	-68.997115	2MASS J04574552-6859495	Can. PAGB			11.633 ± 0.036	749 ± 12	0.44 ± 0.08	113.6	C	12509
74.675126	-68.120909	IRAS 04588-6811	Can. AGB			15.645 ± 0.029	756 ± 19	0.67 ± 0.29	50.4	C	11750
74.678098	-69.280714	IRAS 04590-6921	AGB			17.307 ± 0.058	588 ± 13	0.68 ± 0.25	8.0	C	4320
74.881974	-66.507628	[GC2009] J045931.66-663027.5	YSO			15.191 ± 0.019	514 ± 4	0.46 ± 0.05	41.0	C	2971
74.956396	-75.155069	2MASS J04594953-7509182	Star	C		11.248 ± 0.072	487 ± 4	0.53 ± 0.20	386.3	C	3718
75.134446	-72.150655	MSX LMC 178 2MASS J05003226-7209023	AGB		C(1)	12.698 ± 0.019	547 ± 2	0.67 ± 0.02	30.5	C	6225
75.509936	-69.123936	2MASS J05020239-6907262	Star			12.899 ± 0.042	431 ± 4	0.39 ± 0.03	57.4	C	4815
75.591578	-68.090081	IRAS 05026-6809 2MASS J05022199-6805243	Can. AGB			14.122 ± 0.023	811 ± 5	0.92 ± 0.09	59.5	C	8734
75.685200	-71.658970	2MASS J05024447-7139323	AGB			11.778 ± 0.025	478 ± 3	0.63 ± 0.09	130.7	C	5601
75.893568	-65.807719	MSX LMC 40 2MASS J05033445-6548278	AGB			11.481 ± 0.033	611 ± 9	0.58 ± 0.21	66.6	C	9354
75.910577	-68.886878	IRAS 05038-6857 2MASS J05033853-6853128	AGB			12.998 ± 0.028	952 ± 10	0.78 ± 0.03	72.0	C	12505
75.954591	-66.369916	MSX LMC 38 2MASS J05034910-6622116	LPV			11.008 ± 0.045	615 ± 20	0.29 ± 0.16	148.5	C	10900
75.973947	-64.540777	2MASS J05035373-6432268	AGB			11.501 ± 0.060	434 ± 5	0.53 ± 0.24	336.1	C	4121
76.050010	-69.190646	MSX LMC 105 2MASS J05041201-6911263	AGB			14.051 ± 0.017	473 ± 2	0.66 ± 0.04	19.8	C	3134
76.172007	-71.150449	MSX LMC 151 2MASS J05044128-7109016	AGB			14.919 ± 0.030	549 ± 3	0.80 ± 0.12	67.8	C	5239
76.201387	-64.789768	2MASS J05044833-6447232	AGB			10.896 ± 0.034	482 ± 6	0.47 ± 0.08	167.4	C	8568
76.366322	-68.943236	2MASS J05052791-6856355	Star			12.953 ± 0.027	616 ± 3	0.61 ± 0.08	39.1	C	6424
76.468877	-66.013523	MSX LMC 35 2MASS J05055253-6600486	LPV			11.238 ± 0.061	353 ± 3	0.46 ± 0.11	69.7	C	8642
76.646344	-70.280627	IRAS 05070-7020 2MASS J05063510-7016501	AGB		C(1)	13.315 ± 0.028	555 ± 4	0.55 ± 0.09	99.4	O(AGB)	7032

Table C.2. continued.

RA (deg)	Dec (deg)	Name	Obj. Type	Sp. Type	IRS	K (mag)	Period (d)	Amp (mag)	χ^2_r	SED T	SED L (L_\odot)
76.683469	-69.522966	SAGE1C J050643.98-693122.8	AGB			11.770 \pm 0.031	236 \pm 2	0.24 \pm 0.03	135.9	C	4953
76.684728	-64.704961	2MASS J05064433-6442177	Star			12.247 \pm 0.043	402 \pm 2	0.58 \pm 0.12	89.6	C	4125
76.828770	-68.647341	[GC2009] J050718.89-683850.4	YSO			16.072 \pm 0.036	715 \pm 27	1.04 \pm 0.49	62.6	C	6843
77.246031	-72.165178	2MASS J05085905-7209546	Star			12.069 \pm 0.074	546 \pm 10	0.64 \pm 0.19	392.7	C	5365
77.448975	-68.110454					12.809 \pm 0.045	475 \pm 3	0.68 \pm 0.03	73.6	C	5998
77.466335	-69.042993	2MASS J0509520-690234	YSO			13.409 \pm 0.021	463 \pm 2	0.44 \pm 0.05	16.6	C	3927
77.671774	-68.601841	IRAS 05108-6839 2MASS J05104124-6836066	Star			12.406 \pm 0.041	1089 \pm 11	1.08 \pm 0.08	67.8	C	15828
77.831436	-68.707703	MSX LMC 219 2MASS J0511194-684227	AGB	C	C(1)	12.422 \pm 0.032	720 \pm 7	0.61 \pm 0.08	143.2	C	10078
78.003226	-70.540033	IRAS 05125-7035 2MASS J05120077-7032240	AGB		C(1)	15.313 \pm 0.023	1152 \pm 32	0.47 \pm 0.30	40.4	C	13236
78.066364	-65.311991	2MASS J05121594-6518431	Star			11.193 \pm 0.046	499 \pm 4	0.48 \pm 0.10	163.7	C	7570
78.102208	-67.635157	MSX LMC 269 2MASS J05122453-6738066	AGB			12.333 \pm 0.041	456 \pm 2	0.55 \pm 0.05	50.8	C	5116
78.161438	-64.203811	MSX LMC 11 2MASS J05123875-6412136	C	C		10.767 \pm 0.045	883 \pm 14	0.37 \pm 0.07	276.0	C	17550
78.212659	-69.630639	IRAS 05132-6941 2MASS J05125106-6937502	AGB	C	C(1)	12.430 \pm 0.015	670 \pm 2	0.70 \pm 0.04	37.3	C	8944
78.438873	-69.098944	MSX LMC 227 2MASS J05134534-6905563	AGB			12.202 \pm 0.021	730 \pm 6	0.73 \pm 0.09	35.4	C	12161
78.537126	-64.156927	IRAS 05138-6412 2MASS J05140891-6409248	Star			11.529 \pm 0.057	511 \pm 5	0.51 \pm 0.14	254.7	C	11472
78.561931	-70.069375	2MASS J05141486-7004097	Star			12.942 \pm 0.018	573 \pm 2	0.68 \pm 0.00	44.0	C	4792
78.657903	-68.322487	MSX LMC 225 2MASS J05143787-6819207	AGB			12.014 \pm 0.076	664 \pm 19	0.83 \pm 0.29	346.3	C	11983
78.932355	-70.444909	MSX LMC 208 2MASS J05154376-7026416	AGB			13.165 \pm 0.031	508 \pm 3	0.77 \pm 0.10	114.3	C	5700
79.083599	-70.565582	2MASS J05162005-7033561	AGB			13.433 \pm 0.016	478 \pm 3	0.75 \pm 0.05	33.1	C	4446
79.130749	-71.935574	MSX LMC 425 2MASS J05163138-7156080	AGB			11.348 \pm 0.040	1869 \pm 71	0.27 \pm 0.13	205.8	C	6778
79.189658	-67.726466	2MASS J05164550-6743353	AGB			11.816 \pm 0.151	384 \pm 7	0.20 \pm 0.16	63.9	C	5847
79.252764	-69.325114	MSX LMC 332 2MASS J05170066-6919304	Can. PAGB	PN,		11.061 \pm 0.034	373 \pm 11	0.14 \pm 0.08	48.9	C	10626
79.362279	-68.916247	MSX LMC 349 2MASS J05172693-6854582	AGB	C	C(1)	13.451 \pm 0.047	577 \pm 5	0.73 \pm 0.05	259.7	C	7461
79.549930	-67.298474	2MASS J05181196-6717545	AGB			11.505 \pm 0.035	465 \pm 3	0.33 \pm 0.10	44.6	C	6276
79.765405	-69.492292	IRAS 05195-6933 2MASS J05190380-6929322	LPV			12.144 \pm 0.020	611 \pm 4	0.71 \pm 0.14	102.5	C	14776
79.833805	-69.838951	MSX LMC 371	AGB			11.604 \pm 0.067	1597 \pm 23 ^a	0.80 \pm 0.09	207.4	C	5744
79.925886	-66.455714	2MASS J05194220-6627203	AGB			12.639 \pm 0.033	608 \pm 4	0.73 \pm 0.14	113.3	C	7049
79.929725	-64.556298	MSX LMC 295 2MASS J05194314-6433226	LPV			11.204 \pm 0.031	593 \pm 13	0.29 \pm 0.23	97.0	C	7791
79.975757	-67.661682					11.747 \pm 0.046	496 \pm 6	0.62 \pm 0.16	410.4	C	4832
80.106336	-71.078969	2MASS J05202551-7104443	Star			12.201 \pm 0.020	583 \pm 8	0.43 \pm 0.19	23.2	C	9035
80.159280	-72.851733	MSX LMC 403 2MASS J05203823-7251062	LPV			12.157 \pm 0.038	638 \pm 4	0.65 \pm 0.03	110.4	C	8581
80.436579	-70.129974	2MASS J05214476-7007479	LPV			12.786 \pm 0.015	666 \pm 7 ^b	0.22 \pm 0.05	22.9	C	1182
80.460918	-68.499504	MSX LMC 466 2MASS J05215061-6829581	AGB			15.463 \pm 0.297	843 \pm 14	0.87 \pm 0.13	34.2	C	6652
80.513848	-68.322622	2MASS J05220332-6819214	LPV			12.838 \pm 0.040	895 \pm 8 ^{a,b}	0.38 \pm 0.09	21.8	C	1708
80.745672	-65.734129	2MASS J05225895-6544029	AGB			11.669 \pm 0.026	531 \pm 2	0.64 \pm 0.05	45.1	C	7247
80.802424	-64.158664					10.720 \pm 0.031	449 \pm 3	0.29 \pm 0.08	41.4	C	8455
80.910680	-72.766782	IRAS 05245-7248 2MASS J05233856-7246004	LPV			12.601 \pm 0.028	1358 \pm 12 ^a	0.69 \pm 0.07	36.0	C	13129
80.974746	-71.578871	2MASS J05235393-7134438	YSO			13.176 \pm 0.021	1118 \pm 18 ^a	0.20 \pm 0.04	37.7	O(OTH)	9311
81.029480	-71.961429	MSX LMC 427 2MASS J05240706-7157412	AGB		MA(1)	12.328 \pm 0.026	539 \pm 3	0.58 \pm 0.08	62.8	C	6052
81.085617	-67.535309	MSX LMC 578 2MASS J05242056-6732072	AGB			12.601 \pm 0.027	418 \pm 7	0.94 \pm 0.21	92.5	C	3557
81.098476	-65.536337	MSX LMC 531 2MASS J05242363-6532107	AGB			10.815 \pm 0.043	2125 \pm 65	0.38 \pm 0.18	54.2	C	11138
81.098784	-66.713015	2MASS J05242371-6642468	V			10.472 \pm 0.081	508 \pm 5	0.41 \pm 0.19	387.4	C	9880
81.128347	-69.898115	IRAS 05249-6956 2MASS J05243079-6953533	AGB			11.750 \pm 0.051	739 \pm 19 ^b	0.61 \pm 0.38	272.0	C	29138
81.152682	-72.064715	2MASS J05243664-7203530	LPV			12.352 \pm 0.035	929 \pm 16 ^b	0.38 \pm 0.05	118.3	C	3165
81.161070	-70.399201	MSX LMC 441 2MASS J05243862-7023571	AGB	C	C(1)	13.112 \pm 0.030	668 \pm 6	0.60 \pm 0.16	123.6	C	7364
81.171301	-69.885445	2MASS J05244115-6953075	AGB			13.473 \pm 0.052	613 \pm 15	0.94 \pm 0.21	390.2	C	6711
81.228480	-68.499449					12.276 \pm 0.016	2261 \pm 41	0.20 \pm 0.02	9.3	O(OTH)	1493
81.263672	-69.438127	MSX LMC 484 2MASS J05250325-6926169	Can. AGB			14.375 \pm 0.097	397 \pm 8	0.60 \pm 0.24	282.7	C	4233

Groenewegen et al.: Pulsation periods of enshrouded AGB stars in the Magellanic Clouds

Table C.2. continued.

RA (deg)	Dec (deg)	Name	Obj. Type	Sp. Type	IRS	K (mag)	Period (d)	Amp (mag)	χ^2_r	SED T	SED L (L_\odot)
81.270865	-69.712973	[WSI2008] 657	YSO			12.990 ± 0.038	436 ± 3	0.57 ± 0.09	82.5	C	5068
81.298875	-63.939174	2MASS J05251173-6356209	Star			10.884 ± 0.063	589 ± 17	0.40 ± 0.39	136.1	C	7500
81.596295	-69.188964	MSX LMC 774 2MASS J05262309-6911202	AGB		C(1)	12.374 ± 0.031	669 ± 19	0.91 ± 0.35	150.2	C	7670
81.681240	-66.597920					11.486 ± 0.044	421 ± 5	0.39 ± 0.03	145.0	C	5029
81.795735	-69.570524	MSX LMC 677 2MASS J05271096-6934138	AGB			13.738 ± 0.069	466 ± 5	1.14 ± 0.09	412.7	C	4474
81.839063	-64.377573	[KDM2001] 4130 2MASS J05272137-6422392	C	C		12.356 ± 0.025	441 ± 1	0.79 ± 0.05	32.1	C	3611
81.850469	-69.662488	IRAS 05278-6942 2MASS J05272411-6939449	AGB	C	C(1)	12.934 ± 0.042	997 ± 12	1.25 ± 0.17	142.4	C	25135
81.998815	-69.944145	2MASS J05275971-6956389	YSO			12.416 ± 0.041	683 ± 10	0.64 ± 0.20	245.4	C	4501
82.002315	-72.836662	MSX LMC 694 2MASS J05280053-7250120	AGB			11.043 ± 0.020	518 ± 4^a	0.30 ± 0.05	21.5	C	8779
82.016902	-69.885663	MSX LMC 643 2MASS J05280404-6953082	AGB			12.426 ± 0.034	723 ± 9	0.77 ± 0.22	116.3	C	17625
82.054328	-69.207891	2MASS J05281304-6912283	YSO			12.288 ± 0.033	395 ± 2	0.49 ± 0.07	45.5	C	4330
82.070412	-69.504699	[KWV2015] J052816.85-693017.0	Star			14.500 ± 0.009	592 ± 1	0.83 ± 0.03	5.5	C	7766
82.163018	-67.302460	2MASS J05283913-6718089	AGB			11.794 ± 0.025	494 ± 6	0.61 ± 0.08	103.1	C	7191
82.176406	-69.601943	MSX LMC 659 2MASS J05284234-6936069	LPV			10.127 ± 0.013	588 ± 5	0.14 ± 0.04	0.6	O	15070
82.189710	-70.078809	MSX LMC 656 2MASS J05284552-7004438	AGB			12.633 ± 0.034	656 ± 6	0.74 ± 0.06	174.7	C	7678
82.200664	-71.041372	IRAS 05294-7104 2MASS J05284817-7102289	Mira	M8	MA(1)	9.160 ± 0.032	1078 ± 6	0.73 ± 0.05	8.1	O(AGB)	36906
82.202470	-69.800346	MSX LMC 679 2MASS J05284861-6948013	AGB	C	C(1)	12.534 ± 0.047	481 ± 3	0.39 ± 0.08	88.6	C	4669
82.250906	-69.879886	2MASS J05290019-6952475	Star			12.220 ± 0.012	587 ± 2	0.55 ± 0.07	20.2	C	6616
82.345278	-70.112837	MSX LMC 644 2MASS J05292286-7006461	AGB			13.294 ± 0.036	665 ± 9	1.08 ± 0.25	138.4	C	10197
82.352589	-69.920476	2MASS J05292463-6955136	AGB		MA(1)	11.030 ± 0.069	1263 ± 13	1.18 ± 0.09	239.7	O	20838
82.448330	-68.471978	MSX LMC 605 2MASS J05294760-6828191	Can. PAGB			10.282 ± 0.019	349 ± 2	0.15 ± 0.05	21.0	C	16339
82.491369	-65.839776	SAGE1C J052957.90-655023.2, MSX LMC 842 (?)	AGB			16.396 ± 0.035	674 ± 8	1.25 ± 0.19	27.6	PN	5995
82.516238	-66.823399	IRAS 05300-6651 2MASS J05300389-6649242	AGB		C(1)	12.641 ± 0.017	687 ± 3	0.76 ± 0.04	48.6	C	9176
82.520296	-69.945871	MSX LMC 654 2MASS J05300487-6956451	AGB			13.226 ± 0.042	889 ± 8	0.59 ± 0.15	55.9	C	5473
82.525910	-70.511415	IRAS 05306-7032 2MASS6X J05300621-7030411	AGB		C(1)	15.855 ± 0.014	808 ± 4	0.50 ± 0.04	16.1	C	6319
82.711503	-72.761476	[GC2009] J053050.73-724541.4, IRAS 05318-7247(?)	Can. AGB			16.016 ± 0.016	740 ± 6	0.82 ± 0.08	16.4	C	6652
82.715723	-69.724445	2MASS J05305158-6943263	Star			13.112 ± 0.023	788 ± 7	1.12 ± 0.05	128.2	C	12321
82.804662	-66.161439	2MASS J05311311-6609411	Star		C(1)	11.565 ± 0.047	668 ± 14	0.80 ± 0.18	336.0	C	8929
82.947660	-66.061307	WOH S 374 2MASS J05314741-6603406	Star	M6		8.874 ± 0.029	469 ± 5^b	0.21 ± 0.05	7.1	O	52508
83.005685	-66.057744	EROS2 lm047-6k-20000	LPV			11.706 ± 0.019	504 ± 2	0.57 ± 0.09	80.4	C	5507
83.032126	-64.305241					11.510 ± 0.036	680 ± 9	0.52 ± 0.18	139.2	C	3558
83.146847	-64.406186	HV 996 2MASS J05323561-6755089	RedSG			11.193 ± 0.045	619 ± 9	0.40 ± 0.15	219.9	C	7932
83.154874	-67.115672	MSX LMC 807 2MASS J05323716-6706564	AGB		MA(1)	10.663 ± 0.041	1035 ± 17	0.50 ± 0.22	213.2	O	21458
83.157425	-71.817731	2MASS J05323777-7149037	Star			13.381 ± 0.068	695 ± 6	0.78 ± 0.15	252.5	C	9124
83.213918	-67.114449	MSX LMC 811 2MASS J05325133-6706520	AGB		MA(1)	10.552 ± 0.055	1286 ± 36	0.64 ± 0.22	314.9	O	41277
83.257355	-68.399584	MSX LMC 1780 2MASS J05330176-6823584	AGB			14.132 ± 0.055	410 ± 3	0.55 ± 0.06	234.8	C	13779
83.313626	-67.682367	MSX LMC 880 2MASS J05331527-6740564	LPV			11.536 ± 0.049	543 ± 9	0.65 ± 0.14	290.2	C	6802
83.366343	-68.161155	2MASS J05332794-6809399	LPV			14.038 ± 0.046	773 ± 11	0.62 ± 0.21	170.2	C(AGB)	1002
83.418383	-69.876528	2MASS J05334039-6952355	YSO			13.699 ± 0.016	384 ± 3^b	0.20 ± 0.07	8.4	C	1132
83.566619	-70.381285	IRAS 05348-7024 2MASS J05341598-7022524	AGB		C(1)	12.436 ± 0.024	800 ± 2	0.84 ± 0.03	11.3	C	12859
83.623970	-67.507174	2MASS J05342976-6730257	LPV			10.809 ± 0.027	427 ± 4	0.26 ± 0.08	95.2	C	8210
83.723930	-70.490195	MSX LMC 743 2MASS J05345373-7029247	AGB	C	C(1)	13.001 ± 0.037	547 ± 3	0.67 ± 0.11	182.5	C	8520
83.734170	-69.154601	MSX LMC 787 2MASS J05345621-6909165	AGB		C(1)	12.398 ± 0.050	655 ± 11	0.70 ± 0.14	85.7	C	6352
83.842450	-70.658581	SAGE1C J053522.16-703930.9	AGB			13.078 ± 0.102	395 ± 7	0.55 ± 0.21	415.3	C	4614
84.040121	-67.064856	MSX LMC 873 2MASS J05360962-6703534	LPV			10.359 ± 0.045	653 ± 11	0.65 ± 0.11	8.9	C	9936
84.153318	-70.729275	IRAS 05371-7045 2MASS J05363680-7043455	AGB			12.204 ± 0.042	746 ± 7	0.62 ± 0.14	141.2	C	12319
84.217221	-66.516766	MSX LMC 877 2MASS J05365212-6631004	Can. AGB			11.047 ± 0.013	582 ± 2	0.68 ± 0.04	1.3	C	10019
84.285576	-65.032147	MSX LMC 863 2MASS J05370854-6501557	LPV			10.871 ± 0.085	484 ± 5	0.43 ± 0.18	28.7	C	7905

Table C.2. continued.

RA (deg)	Dec (deg)	Name	Obj. Type	Sp. Type	IRS	K (mag)	Period (d)	Amp (mag)	χ^2_r	SED	SED (L_\odot)
84.937017	-69.921693	IRAS 05402-6956	2MASS J05394488-6955180	Mira		10.236 \pm 0.064	1375 \pm 15	0.94 \pm 0.22	113.8	O	24860
84.986673	-70.537405	2MASS J05395682-7032145	AGB			12.393 \pm 0.029	554 \pm 3 ^b	0.47 \pm 0.09	60.9	C	4121
85.201902	-69.560027	W61 8-88	2MASS J05404850-6933360	Star		7.810 \pm 0.026	576 \pm 5	0.25 \pm 0.03	1.1	O	98601
85.565279	-68.453474	MSX LMC 1396	2MASS J05421566-6827125	AGB		12.410 \pm 0.025	413 \pm 3	0.38 \pm 0.11	77.9	C	5241
85.680518	-71.192689	2MASS J05424333-7111336	Star			13.088 \pm 0.017	530 \pm 3	0.51 \pm 0.11	69.2	C	8642
86.015865	-65.899877	IRAS 05439-6555	Can. AGB			17.528 \pm 0.104	818 \pm 9	1.09 \pm 0.07	7.2	C	9020
86.487337	-72.908108	IRAS 05469-7255	2MASS J05455697-7254291	Star		11.406 \pm 0.025	616 \pm 6	0.99 \pm 0.10	154.5	C	11769
86.935145	-68.644033	IRAS 05480-6839	2MASS J05474446-6838385	AGB		13.468 \pm 0.060	646 \pm 6	0.79 \pm 0.07	159.1	C	5015
87.046488	-70.004655	2MASS J05481114-7000167	AGB			11.924 \pm 0.059	653 \pm 10	0.54 \pm 0.23	319.1	C	4190
87.227457	-72.400368	MSX LMC 1372	Star			14.277 \pm 0.031	517 \pm 3	0.89 \pm 0.05	46.3	C	4535
87.485610	-70.886609	IRAS 05506-7053	2MASS J05495652-7053117	AGB		12.704 \pm 0.079	1019 \pm 18	0.80 \pm 0.14	326.5	C	15378
87.528147	-71.767430	IRAS 05508-7146	2MASS J05500676-7146026	Star		11.426 \pm 0.040	603 \pm 5	0.66 \pm 0.10	106.6	C	7444
87.573225	-64.481849	[KDM2001] 6452	2MASS J05501757-6428545	C		10.687 \pm 0.056	667 \pm 17	0.57 \pm 0.24	221.4	C	8831
87.663857	-67.530692	MSX LMC 1549	2MASS J05503932-6731504	LPV		11.537 \pm 0.045	530 \pm 7	0.25 \pm 0.16	156.2	C	6688
87.708039	-71.393241	IRAS 05516-7124	2MASS J05504991-7123356	Star		13.219 \pm 0.018	666 \pm 4	0.65 \pm 0.08	38.9	C	6625
88.095273	-65.747932	IRAS 05522-6545	2MASS J05522285-6544525	LPV		11.759 \pm 0.036	640 \pm 10	0.69 \pm 0.16	103.2	C	10562
88.111127	-73.421867	EROS2 Im084-0m-19943	LPV			10.799 \pm 0.067	545 \pm 9	0.64 \pm 0.12	6.9	C	7410
88.837681	-70.000864	IRAS 05558-7000	2MASS J05552103-7000030	Mira		9.372 \pm 0.043	1184 \pm 20	0.56 \pm 0.08	18.1	O	26974
89.392127	-75.027369					11.874 \pm 0.044	956 \pm 21	0.48 \pm 0.11	164.3	C	3917
90.629450	-67.213016	IRAS 06025-6712	2MASS J06023105-6712469	C		11.313 \pm 0.080	881 \pm 11	0.56 \pm 0.20	185.9	C	20675
90.676101	-66.528237	2MASS J06024228-6631417	Star			11.555 \pm 0.112	1181 \pm 28 ^a	0.57 \pm 0.13	91.7	C	11992
91.056570	-66.555081	OGLE LMC571.21.04599	LPV			11.954 \pm 0.003	692 \pm 7	0.51 \pm 0.13	1.7	C	6795
91.115156	-67.239721	MSX LMC 1805	2MASS J06042764-6714229	AGB		12.889 \pm 0.068	1258 \pm 12	0.85 \pm 0.06	33.9	C	6917
91.146729	-67.782425	MSX LMC 1699	2MASS J06043522-6746566	LPV		11.586 \pm 0.068	1473 \pm 21 ^a	0.81 \pm 0.20	136.0	C	5742
94.995735	-70.990870	2MASS J06195898-7059271	Star			11.875 \pm 0.029	633 \pm 4	0.56 \pm 0.11	73.3	C(AGB)	4460
96.924335	-68.171171	2MASS J06274183-6810161	Star			11.303 \pm 0.026	600 \pm 5	0.42 \pm 0.12	91.2	C	8285
Most likely not AGB stars or LPVs											
14.875882	-71.522769	2MASS J00593021-7131220	IR			13.648 \pm 0.006	631 \pm 7	0.11 \pm 0.02	5.9	C(OTH)	2480
15.527036	-71.874968					14.293 \pm 0.016	892 \pm 21	0.19 \pm 0.10	35.8	C(OTH)	1244
17.002226	-69.813270					15.103 \pm 0.009	1072 \pm 22 ^a	0.24 \pm 0.07	5.4	Be	531
18.082103	-73.857223	LIN 495 2dFS 2837	Em		B[e]	11.380 \pm 0.045	923 \pm 28	0.33 \pm 0.29	215.3	Be	25870
18.838400	-73.504194	[MA93] 1810	2MASS J01152121-7330151	Em	em	11.351 \pm 0.017	589 \pm 6	0.14 \pm 0.04	18.7	Be(OTH)	53686
20.653925	-73.171293	[MA93] 1895	2MASS J01223695-7310165	Em	em	13.193 \pm 0.032	661 \pm 11	0.20 \pm 0.16	102.3	C(OTH)	2847
72.073972	-68.742486	[WSI2008] 15	2MASS J04481773-6844330	Star		15.106 \pm 0.011	783 \pm 7	0.22 \pm 0.04	7.6	YSO	399
72.333922	-69.227079	2MASS J04492013-6913375	YSO			14.312 \pm 0.014	547 \pm 9	0.13 \pm 0.12	20.3	H II	3519
72.907608	-67.088019	SMP LMC 11	2MASS J04513782-6705166	PN	PN	14.151 \pm 0.013	1740 \pm 22	0.28 \pm 0.04	2.3	PN	14108
72.981613	-70.617580	2MASS J04515558-7037033	Can. PAGB			15.238 \pm 0.034	695 \pm 19	0.34 \pm 0.16	71.7	YSO	741
73.248293	-69.864472	UCAC2 1670938	2MASS J04525958-6951519	Em	em	13.340 \pm 0.012	705 \pm 17	0.14 \pm 0.05	20.0	Be	3468
73.736570	-66.999640	2MASS J04545679-6659586	Can. PAGB			14.681 \pm 0.018	642 \pm 11	0.16 \pm 0.11	15.7	H II(OTH)	1696
73.995435	-75.541192	ESO 33-2 6dFGS gJ045559.0-753228	Seyfert2			11.489 \pm 0.020	737 \pm 12	0.27 \pm 0.19	41.7	YSO(OTH)	20070
74.226760	-68.931631	[RP2006] 1762	Em		F8Ve	14.273 \pm 0.049	979 \pm 39 ^a	0.47 \pm 0.43	231.0	O	619
74.386442	-69.984255	2MASS J04573274-6959032	IR			14.388 \pm 0.026	1073 \pm 10	0.28 \pm 0.04	7.6	YSO	633
74.459013	-66.491599	2MASS J04575016-6629295	Can. YSO			14.639 \pm 0.032	1503 \pm 12	0.85 \pm 0.07	41.6	YSO	2800
76.826621	-68.820270	[WSI2008] 277	YSO			14.372 \pm 0.009	283 \pm 1	0.16 \pm 0.01	12.7	YSO(OTH)	737
77.473769	-68.918522	2MASS J05095369-6855067	YSO			14.578 \pm 0.016	407 \pm 4	0.13 \pm 0.05	4.3	YSO	1242
78.092294	-70.454261	2MASS J05122213-7027152	YSO			14.554 \pm 0.020	356 \pm 3	0.14 \pm 0.06	17.0	H II	1808
78.338631	-65.654077	SAGEMC J051321.26-653914.6	Can. PAGB			13.422 \pm 0.009	741 \pm 4	0.18 \pm 0.02	8.1	Be	1900

Groenewegen et al.: Pulsation periods of enshrouded AGB stars in the Magellanic Clouds

Table C.2. continued.

RA (deg)	Dec (deg)	Name	Obj. Type	Sp. Type	IRS	K (mag)	Period (d)	Amp (mag)	χ^2_r	SED _T	SED _L (L_\odot)
78.776552	-71.652916	2MASS J05150636-7139105	IR			14.435 \pm 0.010	754 \pm 14	0.18 \pm 0.07	5.3	YSO	2285
78.913995	-69.659195	2MASS J05153934-6939330	YSO			14.241 \pm 0.011	713 \pm 5	0.31 \pm 0.05	7.9	YSO(OTH)	885
79.808018	-69.638405	SAGEM A J051913.89-693818.3	Star			12.206 \pm 0.008	1237 \pm 33	0.14 \pm 0.06	10.1	YSO(AGB)	4602
79.926863	-65.038005	2MASS J05194245-6502167, EROS Im045-0n-5960(?)	AGN Can,LPV(?)			14.565 \pm 0.028	1277 \pm 36	0.28 \pm 0.17	17.6	YSO(AGB)	1466
80.692258	-65.682484	[GC2009] J052246.13-654057.0	YSO			15.017 \pm 0.028	890 \pm 9	0.34 \pm 0.02	6.9	H II	2643
82.104224	-64.829461					14.388 \pm 0.075	678 \pm 17	0.68 \pm 0.21	391.9	YSO(AGB)	417
82.115775	-69.001390	2MASS J05282771-6900049	YSO			15.566 \pm 0.017	2542 \pm 55	0.26 \pm 0.04	2.4	YSO	926
82.426783	-68.473434	2MASS6X J05294241-6828244	YSO			14.835 \pm 0.018	602 \pm 8	0.30 \pm 0.13	16.9	H II(OTH)	4570
82.560907	-69.162894	[GC2009] J053014.58-690946.4	YSO			15.612 \pm 0.019	770 \pm 4	0.68 \pm 0.08	9.2	YSO(OTH)	1026
83.332337	-69.695970	2MASS J05331975-6941454	YSO			13.330 \pm 0.014	571 \pm 11	0.14 \pm 0.03	8.0	YSO(AGB)	9360
83.952646	-69.643587	[GC2009] J053548.62-693837.2	YSO			15.477 \pm 0.023	1197 \pm 15	0.19 \pm 0.03	1.6	YSO(OTH)	507
84.519640	-69.988465	[RP2006] 634 2MASS6X J05380473-6959183	Em	B6Ve		15.406 \pm 0.019	1173 \pm 25	0.18 \pm 0.04	0.8	YSO	1329
84.669692	-69.422862					15.043 \pm 0.013	1015 \pm 25 ^a	0.13 \pm 0.04	1.5	YSO	759
85.427863	-71.324496	2MASS6X J05414269-7119282	YSO			14.027 \pm 0.024	1535 \pm 37	0.28 \pm 0.07	19.7	H II	4086
85.432260	-69.627314	LHA 120-S 137 2MASS J05414375-6937383	Em	B:Iaeq		11.299 \pm 0.023	377 \pm 2	0.14 \pm 0.03	11.2	Be	10024
87.229882	-70.086248	2MASS J05485520-7005106	LPV			14.356 \pm 0.006	738 \pm 24	0.11 \pm 0.10	2.6	YSO	7209
89.343232	-67.222617	2MASS J05572239-6713213	LPV			12.899 \pm 0.030	405 \pm 5 ^a	0.20 \pm 0.13	55.4	YSO(AGB)	4510

Notes. Column 1 lists the right ascension and declination of the source in decimal degrees. Column 2 gives some names, copied from Table A.1. Column 3 gives the object type, copied from Table A.1. Column 4 gives the main spectral type, copied from Table A.1. Column 5 gives the main *Spitzer* IRS classification and the reference, copied from Table A.1. Column 6–9 give the mean magnitude, period and amplitude, and χ^2 statistics copied from Table A.3. When a superscript ^a is listed after the period it implies that an alternative period is given in Table A.3. When a superscript ^b is listed after the classification the star is an outlier in the bolometric *PL*-relation (see Fig. 10). Column 10 lists the classification based on the SED template fitting, see Appendix C. Column 11 lists the luminosity of the star based on the template fitting.

This figure "TRGBCMD_BG_ALL.jpg" is available in "jpg" format from:

<http://arxiv.org/ps/2003.04025v1>

This figure "TRGBCMD_LMCbar_ALL.jpg" is available in "jpg" format from:

<http://arxiv.org/ps/2003.04025v1>

This figure "TRGBCMD_WISE_BG.jpg" is available in "jpg" format from:

<http://arxiv.org/ps/2003.04025v1>